University of Windsor

Scholarship at UWindsor

Theses, Dissertations, and Major Papers

December 2022

Machine learning approach to investigate EV battery characteristics

Shayan Falahatdoost
falahat@uwindsor.ca

Follow this and additional works at: https://scholar.uwindsor.ca/major-papers

Part of the Applied Mechanics Commons, Energy Systems Commons, Navigation, Guidance, Control, and Dynamics Commons, Other Computer Engineering Commons, and the Power and Energy Commons

Machine learning approach to investigate EV battery characteristics

By

Shayan Falahatdoost

A Major Research Paper
Submitted to the Faculty of Graduate Studies
through the Department of Mechanical, Automotive and Materials
Engineering
in Partial Fulfillment of the Requirements for
the Degree of Master of Applied Science
at the University of Windsor

Windsor, Ontario, Canada

2022

Machine learning approach to investigate EV battery characteristics

By

Shayan Falahatdoost

APPROVED BY:

_____
N. Zamani
Department of Mechanical, Automotive and Materials Engineering

_____

A. Fartaj, Advisor
Department of Mechanical, Automotive and Materials Engineering

December 8,2022

DECLARATION OF ORIGINALITY

I hereby certify that I am the sole author of this major paper and that no part of this major paper has been published or submitted for publication.

I certify that, to the best of my knowledge, my major paper does not infringe upon anyone's copyright nor violate any proprietary rights and that any ideas, techniques, quotations, or any other material from the work of other people included in my major paper, published or otherwise, are fully acknowledged in accordance with the standard referencing practices. Furthermore, to the extent that I have included copyrighted material that surpasses the bounds of fair dealing within the meaning of the Canada Copyright Act, I certify that I have obtained a written permission from the copyright owner(s) to include such material(s) in my major paper and have included copies of such copyright clearances to my appendix.

I declare that this is a true copy of my major paper, including any final revisions, as approved by my major paper committee and the Graduate Studies office and that this major paper has not been submitted for a higher degree to any other University or Institution.

ABSTRACT

The main factor influencing an electric vehicle's range is its battery. Battery electric vehicles experience driving range reduction in low temperatures. This range reduction results from the heating demand for the cabin and recuperation limits by the braking system. Due to the lack of an internal combustion engine-style heat source, electric vehicles' heating system demands a significant amount of energy. This energy is supplied by the battery and results in driving range reduction. Moreover, Due to the battery's low temperature in cold weather, the charging process through recuperation is limited. This limitation of recuperation is caused by the low reaction rate in low temperatures. Technology developments for battery electric vehicles are mostly focused on maintaining the vehicle battery package temperature and state of charge. For battery management systems, state of charge and battery temperature estimations are important since they prevent over charge, over discharge, and thermal runaway. Estimation and controlling battery temperature and the state of charge guarantees safety, it will also increase the vehicle's life cycle. This study analyzes the effects of ambient and battery temperature on heating system energy demand and regenerative braking parameters. Moreover, different machine learning methods for estimating the battery temperature and its state of charge are compared and presented. The analysis is based on the BMW i3 winter trips dataset which includes data for 38 different drive cycles. Results show that every 3 degrees of ambient temperature drop results in a 1% increase in the heating energy share. Furthermore, the ability of machine learning methods such as LSTM and GRU has been demonstrated to successfully forecast battery temperature and state of charge.

DEDICATION

I dedicate this work to my parents, Mr. Morteza Falahat Doost and Mrs. Parisa Saheb.

ACKNOWLEDGEMENTS

CONTENTS

FIGURES

TABLES

LIST OF ABBREVIATION

EV	Electric Vehicle
Hp-HX	Heat Pump Heat Exchanger
IC	Internal Combustion
BEV	Battery Electric Vehicle
ML	Machine Learning
AI	Artificial Intelligence
SOC	State Of Charge
RNN	Recurrent Neural Networks
LSTM	Long Short-Term Memory
GRU	Gated Recurrent Unit
NiCd	Nickel–Cadmium
NiMH	Nickel–Metal Hydride
ETNN	Electrochemical-Thermal-Neural-Network
NMC	Nickel Manganese Cobalt
HS	The Heating Energy Share
RS	The Recuperation Share

CHAPTER 1

INTRODUCTION

Global warming and greenhouse gas management are controversial issues in the contemporary world and the Transportation industry which mostly relies on internal combustion (IC) engines play a major role in the production of greenhouse gases [1]. IC engines are the main propulsion systems for ground transport, and they are facing serious and increasing challenges due to environmental regulations. It has been reported that more than 15% of CO_2 emissions are caused by the transportation industry [2]. Therefore, some policies have been introduced in recent years in order to reduce greenhouse gas emissions [3]. During these years and due to the problems mentioned electric vehicles have become the main alternative for vehicles with traditional IC engines.

The increasing number of electric vehicles in today's market shows that automobile manufacturers are focusing on the production of electric cars, but it should be considered that electric vehicles have not been popular yet among people in comparison to traditional internal combustion engine vehicles mainly because of the short driving range and fear of leaving stranded without energy before reaching the destination [4-8].

A battery electric vehicle range is mainly determined by 3 elements.

- the amount of electrical energy preserved in the electric vehicle's battery pack

- the electric vehicle's efficiency

- the supplementary power usage, in addition to travel parameters and driving behavior [9].

The first generation of battery electric vehicles which were introduced in the 2010s had ranged from 100 to 150 kilometers per charge, developments that occurred in electric propulsion systems and energy storage systems increased ranges up to 500 kilometers [10, 11]. In this paper, the BMW i3 data are analyzed and estimation models for the battery pack of the BMW i3 are developed.

1.1 BMW i3 Architecture And Driving Data

1.1.1 Heater

Internal combustion engine vehicles can use engine waste heat to warm up the cabin, but electric motors do not produce much heat, so battery electric vehicles need heaters at cooler temperatures to warm up the cabin [12].In cold temperatures, two primary elements will have a strong effect on electric vehicles' range, heating energy demand, and Li-ion batteries' temperature sensitivity [10, 13]. Once the heater is applied to the system, more energy is discharged from the battery which limits the range of the electric vehicles. Heating energy share is a vital factor that should be analyzed by evaluating the heating energy consumption relative to the total power usage of the vehicle. According to Horrein et al. [14], the driving range decreases by 30% at an ambient temperature of 12°C compared to the same drive cycle at 24°C. moreover, Reyes et al. found a range reduction of 70% at an ambient temperature of 15°C in comparison to the same drive cycle at 25°C [15].

1.1.2 Heat Pump

The usage of heat pumps is one way to extend the driving range. Heat pumps use waste heat from the vehicle and ambient heat to warm up the refrigerant, which then

transfers the heat to the cabin. It removes the load on the electric heater and less energy will be consumed. As a result, energy consumption can be reduced by up to 30% [16].

In cold temperatures, the COP of heat pump drops drastically and when the ambient temperature falls below the coolant's freezing point there is a risk of the heat pump freezing, in order to avoid this problem, heat pumps are used in conjunction with an electric heater.

1.1.3 Battery

Battery electric vehicles (BEVs) traveling range is also impacted by the battery's performance. The property of electrolytes is affected by cold temperatures. At low temperatures, the viscosity of the electrolyte increases which will reduce the ionic conductivity. Subsequently, the increase in the impedance of chemical ion transfer will raise the internal resistance of the battery [15-18]. In this regard, Nagasubramanian et al.[19] demonstrated that a Li-ion battery can lose up to 95 percent of its energy and more than 98 percent of its power capacity when exposed to extremely cold temperatures (-40 °C) as opposed to performance levels at 25 °C According to a similar study, a cell's capacity can reduce by up to 23 percent at 20 degrees compared to 25 degrees [20]. Cold temperatures encourage Li-plating, which can cause an irreversible loss of cell performance in addition to these transitory losses.

According to Steinstraeter et al. the capacity of the BEV (Battery Electric Vehicle) to recover braking energy is highly influenced by the temperature of the battery [21]. When a lithium battery is charged at low temperatures a chemical reaction known as lithium plating happens, which is created by the charge flow. It forces the lithium ions to transfer and react at a quicker reaction rate than typical and lithium accumulates on the anode

plate [22]. In comparison to Steinstraeter et al. study that analyzed the recuperation of an electric vehicle, this major paper summarizes and analyzes the contribution of recuperation only in the winter condition [12]. This summarization is c needed since the operation of the electric vehicle systems and potential threats to the battery life are different in winter conditions. Lithium plating and slow charge transfer are the consequences of using BEVs in winter conditions. Moreover, thermal runaway and low resistance of the battery are mostly common in summer driving conditions. In addition to the issues related to the battery during winter and summer conditions, the Electric motor's performance will be different because of the ambient temperature effect on the motor's internal resistance [23].

1.2 Machine Learning Definition

Machine learning (ML) is a type of Artificial Intelligence (AI) that permits computer programs to forecast outcomes more accurately without being explicitly programmed to do so. To predict new output values, machine learning methods use previously extracted data. As well as supporting the development of new products, machine learning provides enterprises with insights into electric vehicle operations [24]. Estimation of the battery characteristics is essential to avoid failure and damage to the battery. This estimation would be more complex since the Heating system drains batteries' energy in the winter when the cold weather influences electric vehicles. In winter conditions, the number of parameters influencing electric vehicle systems will increase, Components such as battery and regenerative braking systems will lose their efficiency and the heating system will require lots of energy to keep the vehicle in operating mode. For improving the driving range, battery life, and battery operational safety, the accurate estimation of the

state of charge (SOC) is necessary [25]. Machine learning methods can be used for the estimation of these complex datasets. They can be used in time series and sequence estimation tasks. Recurrent Neural Networks (RNNs) are a type of machine learning which has several qualities that make it suitable for sequence modeling [26]. The RNNs method can use data from previous events to generate a diverse variety of sequence-to-sequence mappings. RNNs include sets of algorithms for modeling time series data by considering time as a first-class component. Gated architectures in RNN [27] are meant to address the constraints of RNNs by incorporating gating units that are taught to regulate information flow across the network and learn to store data for a long time. In practical uses, both Long Short-Term Memory (LSTM) and Gated Recurrent Unit [28] networks have demonstrated benefits [28-31].

Long short-term memory (LSTM) units or blocks are parts of a Recurrent Neural Networks (RNNs) structure. Artificial memory techniques are created to be used by Recurrent Neural Networks, which can aid these artificial intelligence systems, more accurately mimicking human reasoning. The long short-term memory cell has several parts, including weighted inputs, activation functions, inputs from earlier units, and ultimate results [32]. Long short-term memory is created by combining short-term memory processes with a structure the program calls a long-term memory unit. Recurrent Neural Networks examine specific phonemes within data, where long short-term memory can help sort and categorize these types of input. LSTM is a widely acknowledged and utilized principle in the development of pioneering Recurrent Neural Networks. In comparison to long short-term memory, the Gated Recurrent Unit [28] is a form of Recurrent Neural Networks (RNNs) which is quicker and requires less memory than

LSTM, however, LSTM is much more precise when working with datasets that contain lengthy time series data. Long short-term memory networks have been frequently employed to solve time series prediction problems. Some of these include categorization of multi-sensor anomaly detection [33], forecasting of short-term voltage oscillations in an electric power network [34], estimation of battery state of charge (SOC) [35, 36], diagnosis of charging malfunctions [37] , and forecast of short-term load [38]. GRU, like LSTM, has been effectively used for time series issues. Some of these are wind velocity prediction[39-41], short-term load forecasting in power systems [42], and forecast of Li-ion battery effective life [43]. Two-time time series forecasting models, LSTM and GRU, were utilized in this research to estimate the SOC and Battery temperature for the winter data of the BMW i3 vehicle. The electric vehicle must properly forecast the battery's State of Charge (SOC), which is a major requirement. When a large variety of factors are collected in real-world situations and assessed on the road, predicting SOC is difficult. This study proposes an approach to estimate battery SOC accurately. Some studies have used machine learning methods for battery SOC estimation, for instance, a study used recurrent neural network types and works on 3 battery measures as voltages, current, and temperature to estimate the SOC of Li-ion batteries [36]. The neural network designs utilized in the study are comparable to the ones we investigated in this article [28]. Moreover, the features of the data employed were mainly current, voltage, and temperature. The necessity to evaluate additional sorts of characteristics such as ambient data, driving behavior, vehicle attributes, and the heating system, as well as analyzing their influence on the ability to properly estimate SOC, should be taken to account. In the publication [44], a combination of five ANNs is used to study a mixed estimation of the

SOC and State of Health (SOH): four regression networks focused on SOC prediction and one classifying networks for the state of health recognition. The state of health classification result is employed to choose the optimal SOC prediction from the 4 regression ANNs' findings. In the neural network study, the SOC prediction is employed as an input for the state of health classifier, and the task is only focused on battery characteristics (voltage and current). Recurrent neural network (RNN) types have also been investigated in this study. It also considers the impact of other factors such as the battery, vehicle, and driving behavior.

Despite Li-ion's numerous advantages, the Li-ion battery has one unusual but serious failure scenario for electric vehicles, Lithium plating. This safety issue must be addressed for the Li-ion battery industry to continue to thrive. The majority of Li-ion battery failure scenarios are linked to temperature. Low temperature causes a slow reaction in the cell that decreases ion conductivity and forced ion movement, leading to lithium depositing on the anode. Therefore, it is critical to keep the temperature at a specified threshold to avoid battery failure caused by temperature deviations. As a result, checking battery temperature is critical for avoiding battery malfunction. Several temperature sensors are now used to check the temperature of the battery cells in electric vehicles (EVs). The quantity of temperature sensors used to check the battery pack rises as the capacity of the battery pack increases and the cells are densely packed to achieve higher energy density [45]. Furthermore, having more sensors increases the likelihood of sensor failure, which inhibits accurate temperature measurement and increases maintenance costs and customer concerns. There are multiple studies that focused on battery temperature estimation using different methods. The following study proposed replacing thermal sensors with a

temperature estimating algorithm while keeping accurate temperature monitoring performance. Temperature estimates may be done in a variety of methods. Ralph E. White et al. and Chee Burm Shin et al. have also developed a theoretical temperature with respect to battery chemistry [46, 47]. However, simulation and theoretical modeling provide a decent temperature estimate, direct usage of simulation outcomes for continuous temperature tracking is nearly impossible, and developing theoretical models for a variety of batteries is complex. Additionally, computer simulation provides far more detail than is necessary.

The Artificial Neural Network model was developed by Ala Hussein et al. to predict the temperature of different types of batteries including Li-ion, NiCd, and NiMH [48]. To forecast battery temperature and battery voltage, Feng et al. [49] employed a lumped thermal analysis. To improve the results of the selected models, a neural network was added, resulting in an electrochemical-thermal-neural-network (ETNN) model. This study mixed lumped analysis with a machine learning approach. In contrast with this study, electric vehicle battery temperature is subjected to the effects of different parameters such as cabin temperature, heating circuit, and driving behavior. Due to the importance of mentioned parameters, our study considers all of them. A study presents the temperature estimation approach for electric vehicle Li-ion batteries in a semi-transient case study [45]. The study used the extreme learning machine technique and multi-lumped-state thermal model for battery temperature estimation and compares both methods.

1.3 Objective Of The Research

Over the years electric vehicles have become a popular type of transportation but they have faced many difficulties in different environmental situations. It is evident that electric vehicles are not as reliable as internal combustion engine vehicles. Maintaining battery packages of electric vehicles can be a solution going forward for overcoming environmental situations such as extreme cold. Despite numerous works on sole analyses of the electric vehicle's battery packages from various points of view, there haven't been enough studies focused on heating and recuperation analysis in vehicles to discover the effects of ambient and battery temperature in winter conditions. The further aspect of this work is the development of recurrent neural networks to estimate battery state of charge and temperature, by the utilization of python programming language and google colab as an integrated development environment for python programming. The analysis in this major paper attempts contributing to the missing work. The main objectives of the current study are included below:

1. To analyze the effects of ambient temperature on heating energy demand
2. To analyze the effects of battery temperature on recuperation
3. To develop & compare battery state of charge estimation models
4. To develop & compare battery temperature estimation models

CHAPTER 2

BMW I3 ARCHITECTURE AND DRIVING DATA

The battery and heating data in real driving cycles dataset is used in this study [50]. In order to parameterize and verify the model for this research, a driving dataset from the BMW i3 was acquired [50]. The vehicle data was measured and recorded using CAN bus system signals and Information was collected by Vector CANoe software. The electrical system which makes communication within the different electrical parts of the vehicle is called Controller Area Network (CAN bus) [51]. The CAN bus connects "nodes" or "Electronic Control Units" (ECUs). Each electrical part of the vehicle in the CAN bus system is considered to be a node or an ECU. In modern vehicles, the word "ECU" refers to the equipment that controls the electrical systems and transmits commanding messages to the nodes and then nodes will act accordingly. which are similar to organs in the body. One component transmits messages and the other one receives those messages. ECUs include the engine control unit, airbags, stereo system, and other components in an automobile CAN bus system. Approximately 70 ECUs may be present in a contemporary automobile, and each one of them may have data that has to be exchanged with other devices in the network [51].

With the test vehicle, 72 travels (= 1514 km) were documented in two parts.

- Part A: data is documented during summer in warm weather.

- Part B: data was recorded in a cold environment during the winter season.

The same driver who had consistent driving habits drove on all trips. Before driving, the car was left outdoors to confirm that the coolant fluid and battery temperatures were roughly equal to the outside temperature.in addition, The interior ventilation was always in automatic mode and set at 21 °C.

For each trip the following data was employed:

- Environmental data (temperature, elevation, etc.)

- Vehicle data (speed, throttle, etc.)

- Battery data (voltage, current, temperature, SOC)

- Heating circuit data (cabin temperature, heating power, etc.)

The battery temperature ranged from -1.5 °C to 32 °C during winter and summer trips. The SOC fluctuated from 15.4% to 88.5% at the beginning of the trips and the driver saw the upper limit as being completely charged. This dataset came from road tests related to BEV studies at the Technical University of Munich (TUM)'s Institute of Automotive Technology (FTM). Nine of the trips were recorded on FTM route and they are quite similar to each other. Table 2.1 shows the different properties such as cell chemistry and weight of the BMW i3 [50, 52].

Table 2.1 Properties of BMW i3

Property	BMW i3
Vehicle mass in kg	1195
Drag coefficient	0.29
Rolling resistance coefficient	0.008
Cross-sectional front area in m2	2.38
Max. power in kW	125
Drive topology	Rear Axle—Single Motor
Machine type	PMSM
Gearbox type	Two-Stage Spur
Total gear ratio	9.7
Tire size	175/60 R19
Dynamic tire radius in m	0.336
Powertrain moment of inertia in kg·m2	10.42
Battery size (gross/net) in kWh	22/18.8
Cell chemistry	NMC
Heater	Layer

BMW i3 uses a single Permanent Magnet Synchronous Motor (PMSM) on its rear axle. The Permanent Magnet Synchronous Motor (PMSM) is an AC synchronous motor that is a hybrid of an induction motor and a brushless DC motor which consumes energy up to 125 kW [25]. According to table 1, this vehicle is a relatively light and super compact vehicle with a high power 125 kW traction motor Table 2.2 summarizes the distance, duration, battery state of charge changes, and battery temperature variation in each trip.

Table 2.2 Winter Trips Summarized Information

Trips	Battery temperature start-end °C	Battery state of charge change %	Ambient temperature °C	Distance km	Duration min
B01	7-15	28.7%	8.5	38.79	54.20
B02	13-15	14.8%	6.5	18.93	26.85
B03	9-12	17.0%	3.5	19.40	26.32
B04	12-20	-24.1%	9.0	16.60	49.25
B05	10-11	12.4%	7.0	14.82	16.99
B06	11-13	13.9%	6.0	16.58	22.53
B07	5-8	17.0%	2.5	30.38	38.16
B08	7-10	23.3%	3.5	32.22	48.57
B09	0-14	24.0%	5.5	54.18	93.50
B10	2-14	45.8%	2.5	47.84	33.72
B11	14-15	8.1%	4.0	10.21	12.56
B12	22-20	22.1%	7.5	37.06	53.76
B13	20-20	1.9%	6.0	2.78	5.91
B14	3-13	50.9%	3.0	60.97	63.70
B15	9-11	17.6%	2.0	19.24	30.37
B16	11-13	14.7%	3.0	19.23	25.48
B17	13-15	15.6%	3.5	19.25	26.02
B18	3-6	14.7%	2.5	15.81	18.49
B19	6-8	14.2%	3.0	16.43	19.85
B20	10-12	10.7%	5.0	12.34	23.38
B21	7-9	14.6%	1.5	15.84	17.33
B22	11-13	13.9%	7.5	16.86	19.99
B23	6-10	18.6%	5.0	18.71	18.55
B24	10-11	7.9%	6.5	9.33	16.30
B25	10-12	11.8%	5.5	13.50	17.03
B26	12-15	12.2%	5.5	14.70	13.42
B27	1-5	18.4%	1.0	19.23	24.48
B28	5-10	14.4%	3.5	17.53	22.77
B29	11-14	16.1%	3.5	15.83	16.14
B30	4-6	13.8%	0.0	14.86	15.35
B31	6-8	14.3%	3.5	15.24	18.28
B32	4-7	14.5%	2.0	14.24	13.26
B33	11-12	5.8%	4.0	7.03	9.13
B34	11-11	2.6%	5.5	9.14	12.23
B35	11-13	13.9%	4.0	15.42	22.71
B36	6-10	27.6%	4.0	38.72	47.54
B37	8-10	15.8%	-3.0	17.46	23.62
B38	-1- 3	16.2%	-1.5	18.90	27.38

In all of the drive cycles, the battery has lost energy but in drive cycle 4 the vehicle charged up by 24%. This driving cycle includes the driving and charging process which is shown in figure 2.1.
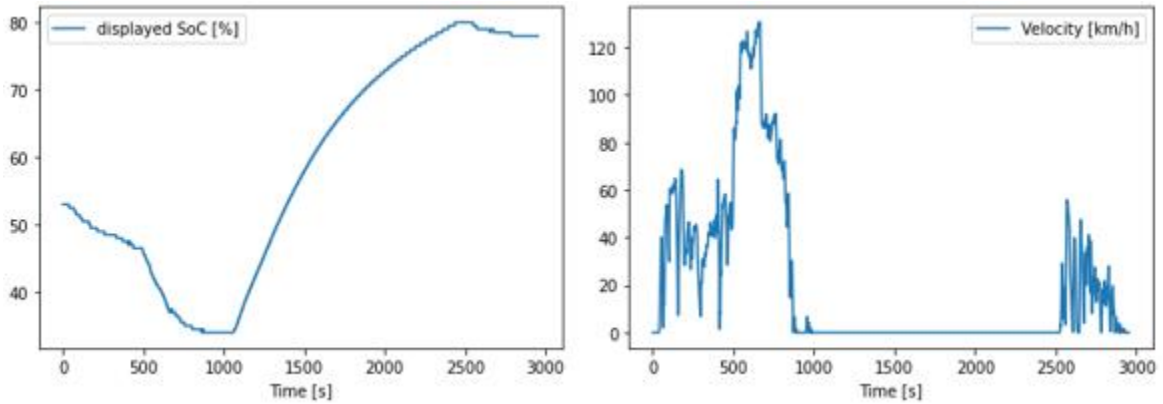
Figure 2.1 Displayed SOC & Velocity Chart of Drive Cycle B04

In drive cycle 4 battery charges up by the fast charging. The driver drove the car for about 1000 seconds and starts charging the car for about 1500 seconds. **Figure 2.1** illustrates the velocity profile of Trip B04 with a mean velocity of 20.21 km/h. **Table 2.3** shows the number of recorded trips in the winter and their total traveled distance. Moreover, two major factors such as the ambient temperature range of the winter drive cycles and the battery temperature range are included.

Table 2.3 General Winter Data Summarized

Property	BMW i3
Number of trips in winter	38
Distance in km	780.81
Ambient temperature range in °C	-3.0 - 9.0
Battery temperature range in °C	-1.5 - 22

Based on the table, winter trips have the ambient temperature range between -3.0 °C to 9.0 °C. This temperature range shows that the tests were recorded in a mild winter temperature.

2.1 Heater

The resistive heater in the BMW i3 is a layer heater with a nominal power usage of 7 kW. Figure 2.2 shows a layer heater.
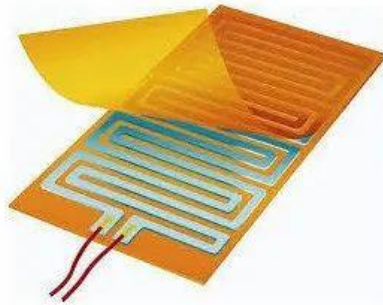
Figure 2.2 Layer Heater[53]

The heater is responsible for warming up the coolant and letting the hot coolant transfer the heat to different sections of the vehicle. In the winter, the heater starts working when the vehicle turns on, and it will reach its maximum power consumption very fast, this behavior will unfreeze the heat pump heat exchanger and increase its COP, and after a while, the electric heater energy consumption will be reduced and stabilized. An analysis of heater usage at a low temperature is included below. Table 2.4 presents the key parameters of the resistive heater used in the BMW i3 vehicle.

Table 2.4 Key Parameters of Heater [54]

Heater Parameters	Value
Nominal power	7 kW
Peak power (overload)	20 kW
Mass	1.89 Kg
Specific heat capacity	866 J/ (Kg K)
Heat transfer coefficient	190 W/K

The nominal power, Peak power, mass, heat transfer coefficient, and specific heat capacity of the heater are included.

- Heating analysis:

    To find the effect of heating on the vehicle's range, the power consumption of the BMW i3 was examined. Heating share is a coefficient that can show the effect of heating energy on electric vehicles. The heating energy share (HS) is the energy consumption of the heater over the total battery consumption [25]. Heat share was calculated by current and voltage which are recorded inside the electric heater and battery packs.

The thermal assessment is covered in the heater part, while the regenerative braking evaluation is covered in the battery. An assessment in one stage is carried out in both parts. A broad, theoretical approach to the relevant topic is done at the start of each part. This part analyses the power fractions of heating and battery part analyzes regenerative braking recovery for all trips in the dataset and draws conclusions about ranges from the results. The battery pack temperature depends on regenerative braking energy limits were also discovered as part of the overall recuperation assessment.

2.1.1 Heating Energy Share

Equation 1 shows the consumed energy in each trip without considering the effect of regenerative braking.

$$Heat\ Share = \frac{\int_0^t I_{Heat} * V_{Heat}\ dt}{\int_0^t I_{Battery\ discharge} * V_{Battery}\ dt} \qquad (1)$$

The battery power usage is shown by the integration of battery discharge current and voltage. The heating share equation uses the heater energy usage only in order to separate the effects of heating from the effect of regenerative braking on the vehicle energy usage and vehicle range. The calculated share immediately correlates with the large reductions in the vehicle's range caused by heating throughout the trip since it represents the relationship between a trip's total energy consumption and the energy share needed for heating and ventilation in each of the trips.

2.2 Heat Pump

Using a heat pump can extend the electric vehicle range. Unlike resistive heaters, heat pump's coefficient of performance is higher than 1 [4]. The heat from ambient and excess heat in the vehicle is absorbed by the refrigerant and it will evaporate then the refrigerant will be heated by compression. The heat will be directed to the condenser by the heated refrigerant and heat will be transferred to the cabin or the coolant. The heat pump system can reduce energy consumption by 30% [55]. The heat pumps are used in combination with a resistive heater in order to avoid heat pumps freezing and having low COP due to low temperature.

The studied vehicle (BMW i3) has three types of circuits that will allow vehicle heating and ventilation to be suitable for every environmental condition. Heating, cooling and mixing circuits of the thermal model.

2.2.1 Heating Circuit

The vehicle circuit model is developed by Wagner et al. [56]. Figure 2.3 illustrates the heating circuit of the BMW i3 with all its components and flow directions. The arrow in the schematic shows the direction and the red and blue colors show the warm and cold fluids accordingly. Closed or non-operating parts are colored gray. The Circuit schematic comprises several main components. Heat pump heat exchanger (HP-HX), Coolant expansion tank, resistant heater, expansion valve, one-way valve, compressor, shut off valve, fan, heater core, pump, Battery, heat pump evaporator, and heat pump condenser. Figure 2.4 shows the symbols of each component in the schematics.
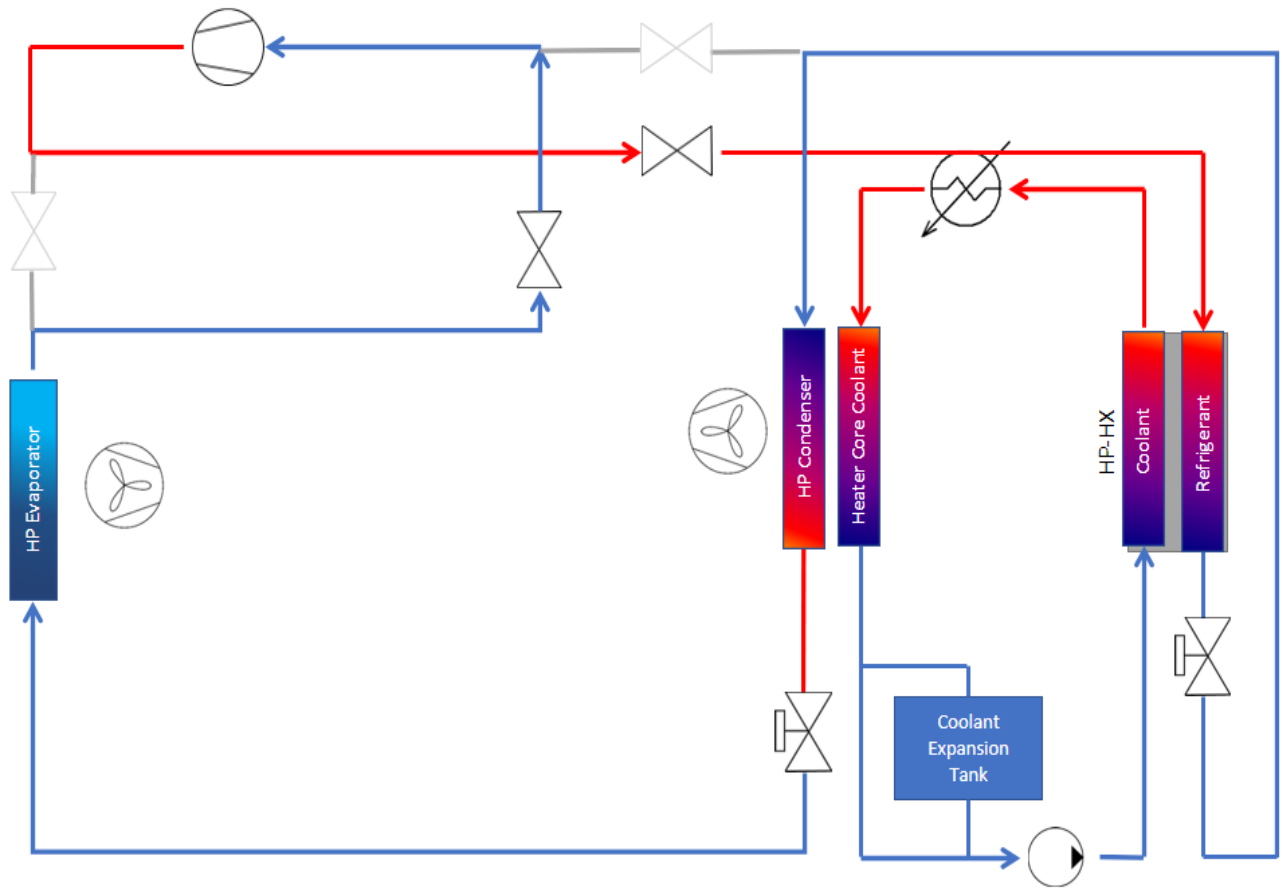
Figure 2.3 Heating Circuit[57]

Figure 2.4 Symbols and Components

In the heating circuit, the coolant is heated by the resistive heater and heat pump heat exchanger and then transfers heat to the heater core. The fan will create forced convection and transfers heat from the heater core to the heat pump condenser and passenger cabin. The heat pump heat exchanger is a component with 2- sides, a coolant

and refrigerant side which will heat the coolant and reduce the load on the resistive heater. The refrigerant shut-off valves direct the refrigerant flow to the heat pump heat exchanger. Grey-colored shut-off valves are the closed valves that allow the refrigerant to flow through the heat pump heat exchanger. The refrigerant pressure increases by the electrically controlled expansion valve after the heat pump heat exchanger aim to heat the refrigerant. The evaporator is also a component that has an electrically controlled expansion valve before it. The expansion valve builds up pressure and raises the heat in the refrigerant before reaching the evaporator. Table 2.5 presents information about the BMW i3 heat pump system. Table 2-5 includes the tube length of the electric heater to the heater core and vice versa, tube diameter, air mass flow inlet, and coolant and cabin data.

Table 2.5 Heat Pump Data [54]

COMPONENT/FLUID	PARAMETER	VALUE
TUBES	Length Tube 1 (EH-HC)	0.5m
	Length Tube 2 (HC-EH)	2m
	Inner diameter	20mm
	Specific heat capacity	2100 J/ (kg K)
AIR	Max. Mass flow (Entering vehicle)	300 kg/h
COOLANT	Mass flow	522 kg/h
	Max Temperature	70°C
CABIN	Total surface	15.23 m2
	Heat capacity	65 kJ/kg

2.2.2 Mix Circuit

Figure 2.5 shows the mix circuit and the components.
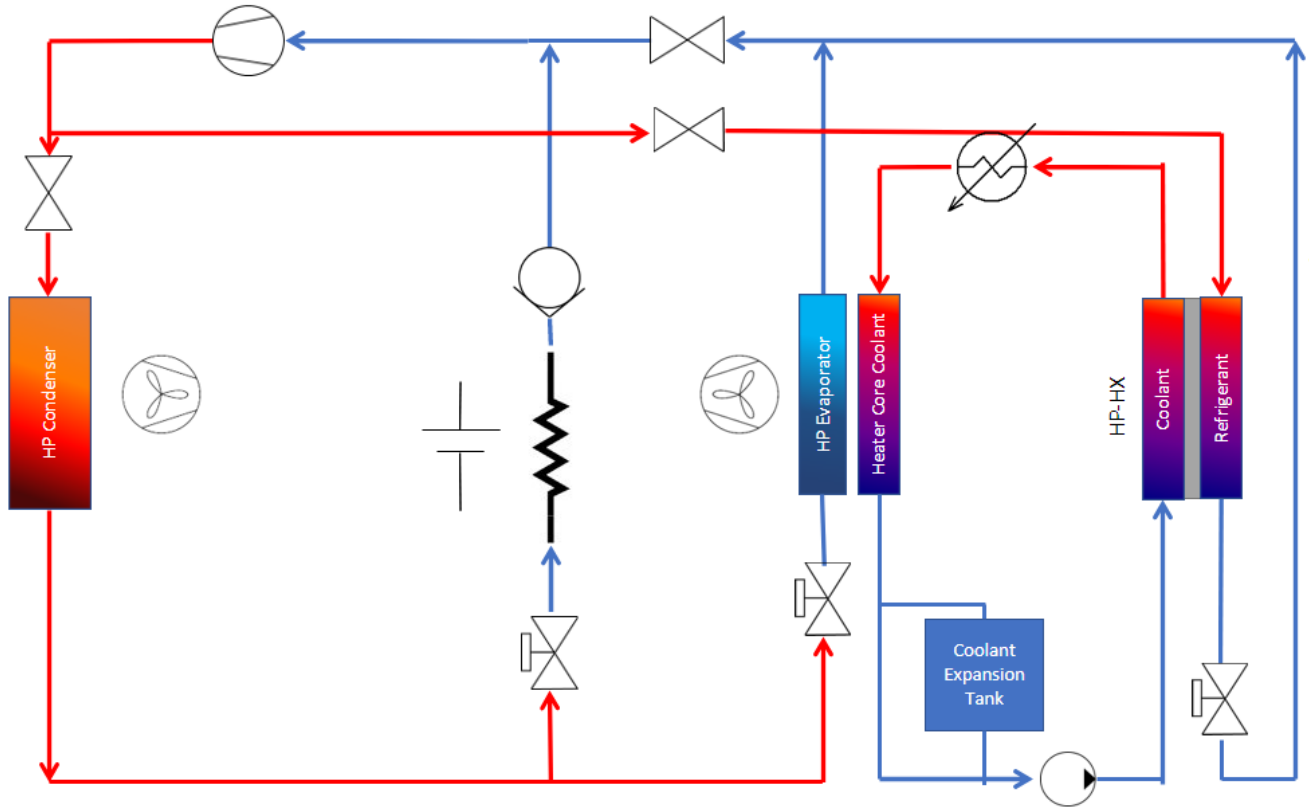
Figure 2.5 Mix Circuit [57]

In the mix circuit, the heated refrigerant after the compressor will be divided and enter the heat pump heat exchanger and heat pump condenser. The roles of heat exchangers swap in the mix circuit, the heat pump condenser act as a heat pump evaporator and vice versa. This switch between the condenser and evaporator, which enables the dehumidification of the vehicle interior, is the main difference between the mix circuit and the heating circuit. Passenger cabin cooling and dehumidification are done by the evaporator. The battery cooling is controlled by an expansion valve. A resistant electric heater is responsible for heating the battery [58].

2.2.3 Cooling Circuit

Figure 2.6 shows the cooling circuit. The cooling circuit does not include the coolant side and it is a simple heat pump system. The battery is cooled with the help of the expansion valve located before the battery circuit.
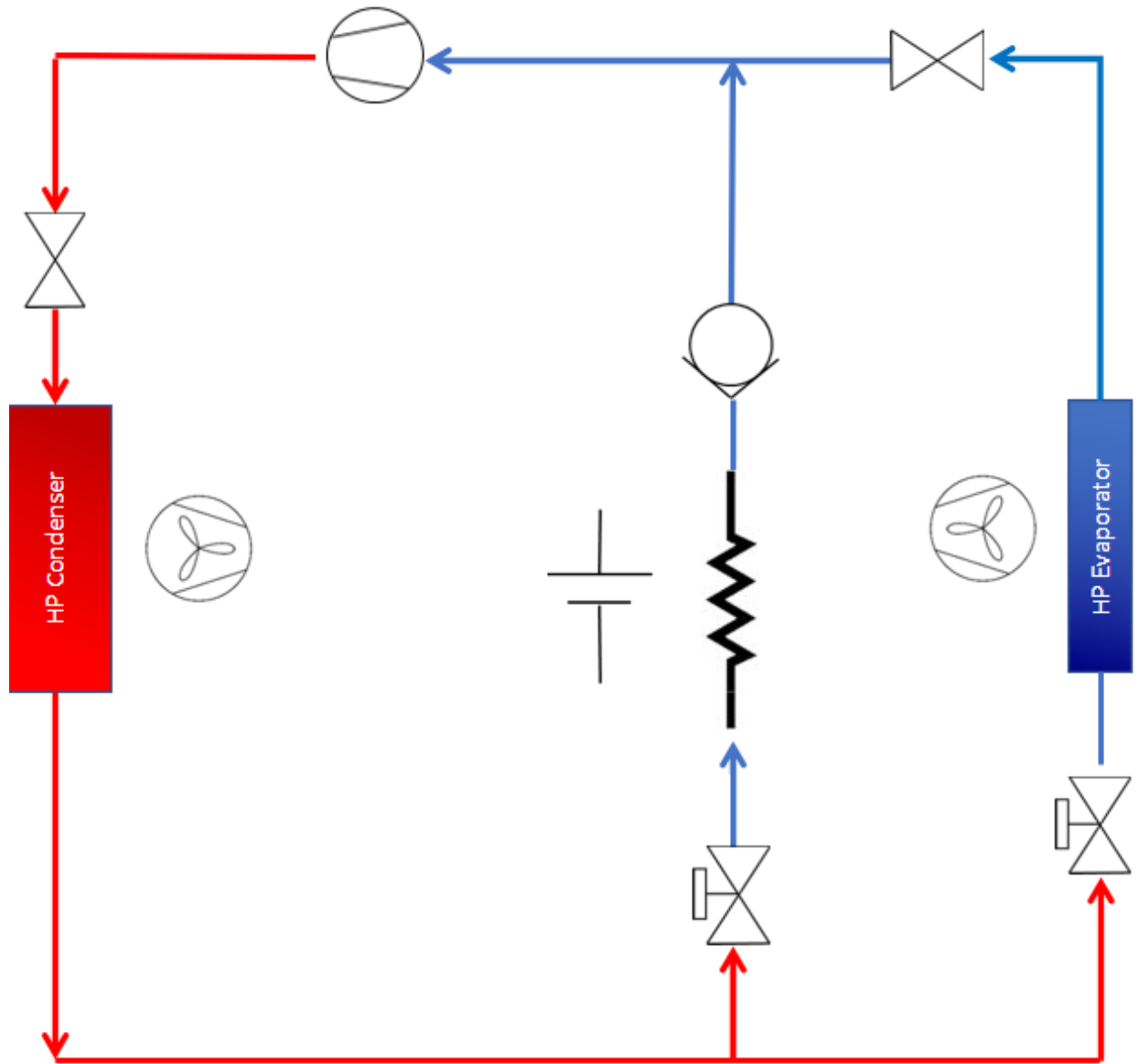
Figure 2.6 Cooling Circuit[57]

2.2.4 Battery Heating/Cooling

Figure 2.7 shows the battery heating cooling system. The heating/cooling system of the battery has a complicated structure. It consists of a grid that has eight flat aluminum tubes of 2mm thickness. These tubes control 8 modules' temperatures. There is a high-voltage heating strip that is fixed on each flat tube, and the duty of this strip is to heat the battery. The electric vehicle's body is constructed of lightweight materials and the Li-ion battery is located at the bottom of the vehicle. Due to the carefully considered and planned design, there was a possibility of placing an HVB with a capacity of 22 kW * h with a voltage of 360 V, which allows the vehicle to travel 130-150 km with a fully charged battery [58].

Figure 2.7 Battery Heating/Cooling System [58]

2.3 Battery

The Li-ion battery used in the BMW i3 is made of a mixture of lithium manganese oxide and nickel manganese cobalt (NMC) and this nickel manganese cobalt mixture is used in the cathode [2]. The battery package is in the 96s1p (96 cells in series and 1 in parallel) layout which provides about 403 volts at max and a nominal voltage of 360 volts. The battery package has a capacity of 60 Ah and a gross battery capacity of 21.8 kWh. The operating range of the battery package SOC is between 8% to 88.6% 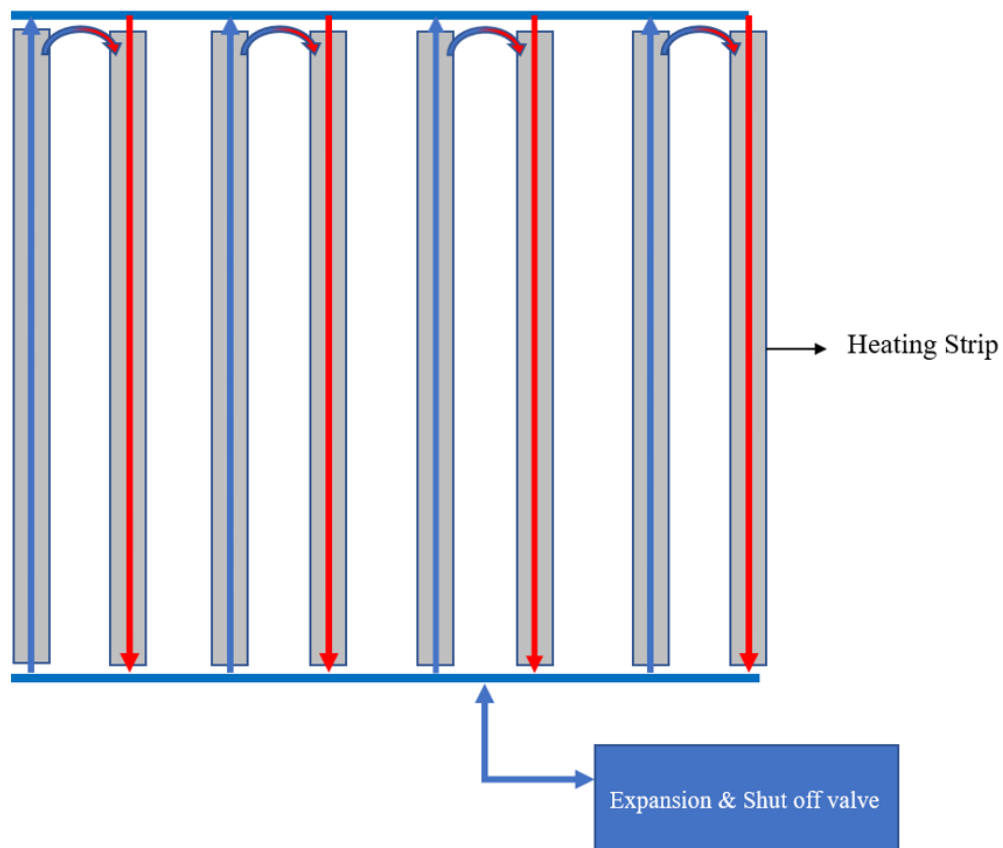of the total battery capacity [25]. Li-ion batteries have a standard operational temperature, these batteries should not work in low temperatures because the viscosity of electrolytes increases, and the charge transfer rate will be slower than usual. This low charge transfer rate damages and reduces the energy and power capabilities of the battery package. One of the effects of low temperature on the battery is the lithium plating. Lithium plating is a phenomenon occurring under the charging process in low temperatures. Lithium particles move and deposit on the anode of the Li-ion battery and will cause damage to the battery. In the charging cycle, lithium ions from the cathode are diffused into mixtures within the anode. Lithium plating happens in this process, which is called intercalation. There are two main reasons for lithium plating. The first one is the high charging current which forces ions to travel at a higher speed and deposit on the anode surface. The second reason is the low-temperature charging which slows down the reaction process and affects the intercalation process. Figure 2.8 shows the lithium plating phenomenon with positive lithium ions accumulating on the anode of the battery.
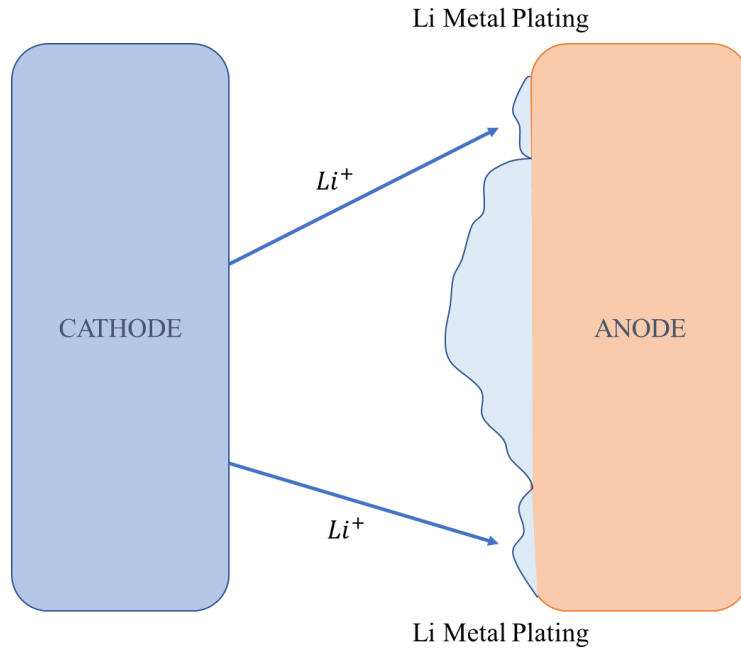
Figure 2.8 Lithium Plating [59]

According to figure 2.9, the BMW i3 battery temperature wasn't in the suitable range of 15-35 C most of the time [60]. This figure shows the battery temperature distribution of all trips in the winter which shows the high chance of lithium plating and the lack of an efficient battery thermal management system in the BMW i3. The regeneration of energy using the braking system is a charging method that can heavily affect the battery. high charging currents will damage the battery when the vehicle is decelerating. Moreover, the slow charge transfer is affecting the charging and performance of the regenerative braking, thus an analysis regarding the recuperation and the effect of battery temperature on the recuperation should be done [59].
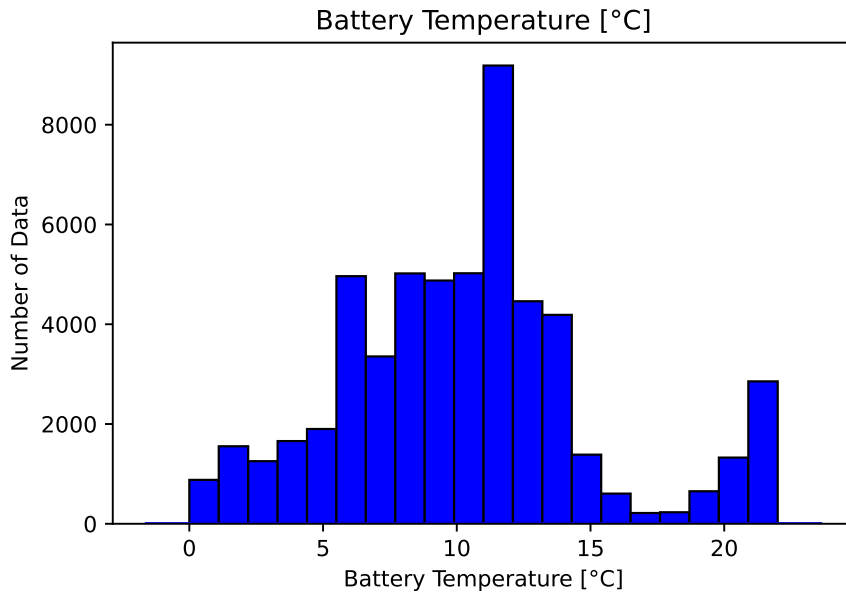
Figure 2.9 Battery Temperature Density

Based on figure 2.9, the vehicle's battery is mostly operating in the temperature range of 5 to 15 C. Figure 2-10 shows the powertrain structure of the BMW i3. This low temperature causes an internal resistance increase in the battery.
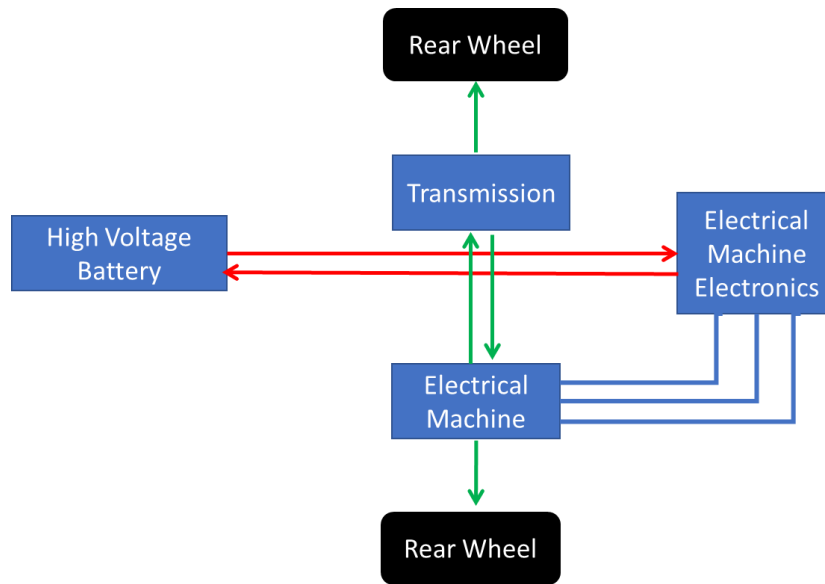
Figure 2.10 Battery Temperature Density

According to figure 2.10, a high voltage battery powers the electrical machine electronics and the machine electronics feed the electrical machine with 3 phase electricity. The power generated by the machine will be transferred to the transmission and then to the wheels. Charging using regenerative braking is carried out by creating negative torque in vehicle movement direction. This negative torque or resistance to movement is created by the electrical machine. By negative torque, an Electrical machine produces electricity and then this electricity is regulated and then charges the battery [57].

- Recuperation analysis:

  The energy demand for each trip was examined in order to determine how recuperation might affect the BMW i3 energy usage and range. Recuperation energy share (RS) is the energy generated by regenerative braking over the overall energy consumption excluding heating energy consumption [25].

The thermal assessment is covered in the initial part, while the regenerative braking evaluation is covered in the second. An assessment is carried out in both parts. A broad, theoretical approach to the relevant topic is done at the start of each part. This section analyses the power fractions of heating and regenerative braking recovery for all trips in the dataset and draws conclusions about ranges from the results. regenerative braking energy generation depends on the battery pack temperature. Which was also discovered as part of the overall recuperation assessment.

2.3.1 Regenerative Braking Energy Share (RS)

$$RS = \frac{\int_0^t I_{Battery\ Charging} * V_{Battery}\ dt}{\int_0^t I_{Battery\ Discharge} * V_{Battery} \quad - \quad I_{Heater} * V_{Heater} \quad dt} \qquad (2)$$

Like the heating share formula, the influence of regenerative braking on the BMW i3 driving range and power usage is calculated by studying each trip's power demand and energy regeneration. Unlike the heat share formula, the traction system power was used instead of total energy consumption. Since the effect of heating energy is not involved, the equation will be able to isolate and evaluate the effect of regenerative braking on the total vehicle traction power consumption and vehicle range. Regenerative braking share shows the energy regeneration of braking over the total power usage of the traction system for each trip. Recuperation share presents the contribution to range increase through regenerative braking in a trip. Due to the low temperature, the regenerative braking effect will deteriorate. The range gain will be reduced in low temperatures compared to the same trip in a warmer climate. Since the Heating effect is not taken into account, this calculated range reduction will be an isolated theoretical approach.

CHAPTER 3

MACHINE LEARNING

Machine learning is a growing field in computer science that is developed to imitate human intelligence and learning from nature. Machine learning is considered as a practical and useful tool in the field of data science. Machine learning methods are being applied successfully in a variety of fields such as computer vision, finance, engineering, entertainment, mechanical engineering, and automotive applications [24]. The complexity of machine learning methods differs from each other and each of them includes multiple levels of sophisticated human-machine interactions. Machine learning methods have the ability to optimize and automate processes. Machine learning methods have the potential to learn from available data and implement learned knowledge on unseen tasks in order to solve problems. A machine learning method is a computational process that employs some data as input and also it tries to finish a duty without being instructed by programming (hard coded). The machine learning methods change and adapt their architecture with repetition in order to improve themselves in performing the required duty. The adaptation process is called the training process. The sampled input data is supplied along with the preferred output. The machine learning method forms itself optimally in order to produce the desired results not only when it is operating with training inputs but also when it receives unseen input data. Training is the learning process in machine learning. Training is not restricted to the initial adaptation of the model in a finite iterating period. A decent algorithm can learn in the lifelong process Like humans. The input data can be chosen and weighted to deliver accurate outcomes. The machine learning method has variable parameters which are altered by optimizing

iterations. It can define probability distributions using inputs and employ them to estimate the output. Ideal machine learning is to mimic the human learning process by receiving inputs in order to reach a goal. The aim of machine learning can be pattern recognition to distinguish bananas from strawberries. Every fruit is distinctive, and it can be identified easily. Instead of hard code software with lots of definite representations of each fruit, a Machine learning algorithm can learn to distinguish them by using repeated learning iteration with actual strawberries and bananas. This process is a decent example of supervised learning. Supervised machine learning uses paired known inputs and known outputs, for instance, input features such as color, and shape is paired with known classified labels such as strawberries and bananas. This learning method permits the algorithm to use similarities and differences with known input-output pairs to classify unknown outputs [61]. Unsupervised learning is the other variety of machine learning. Unsupervised learning, also known as unsupervised machine learning, uses machine learning algorithms to analyze and classify unlabeled data. The users don't have to supervise the model. Instead, it allows the model to work on its own and discover new information and patterns. It mostly addresses unlabeled data. Without the intervention of a supervisor, these algorithms discover hidden patterns or information clusters. It is the best option for data exploration, and image identification because it can highlight patterns and contrasts in information [62]. Semi-supervised learning, in which some of the data is labeled and some of it is not, is the third form of machine learning. In this case, the labeled portion can be utilized as the unmarked portion learn [63]. This sort of environment lends itself to the majority of natural processes and more closely resembles how humans learn new abilities. New insights into comprehending the behavior of

complex systems have been provided by neural network-based system modeling and identification tools. Artificial neural networks are created in an effort to replicate the functionalities that a human neural network can perform, such as learning adaptation, generalization, massive parallelism, robustness, associative storage of information, and spatiotemporal information processing, based on the anatomy of the human nervous system and the mechanism of its operation. There are two key problems that need to be resolved similar to those in many systems identification models.

- The proper selection of neural network architecture (such as model parameters, activation functions, and connection types)
- The choice of model training algorithms

The artificial neural network is designed to emulate the structure of the human brain's neural network and to simulate how it functions. The human brain is a vast and extremely sophisticated neural network. Figure 3.1 shows a biological neuron network with a single neuron cell as an example. The biological sensory organs may be of different sorts, the input signals are all captured by the cell dendrites then the neurochemical impulse (also called stimulus) is transmitted through axons to the axon terminals (in a unilateral pattern). The axons of each neuron are connected to their dendrites and exchange nerve information in a synapse. A human brain contains 100 billion neurons on average. The neural network can handle more sophisticated information as more neurons participate in the process.
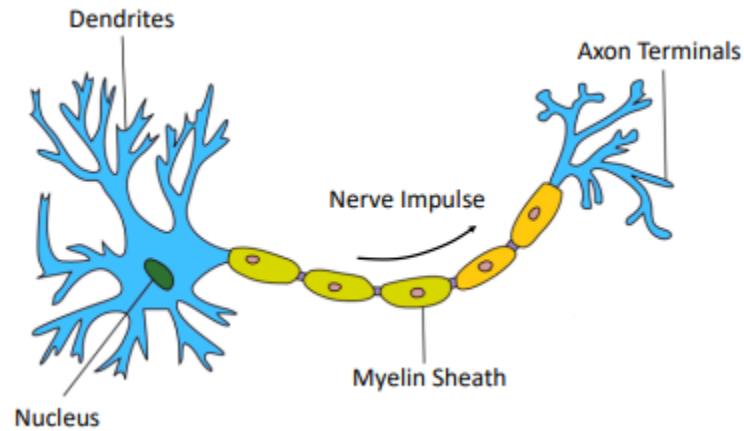
Figure 3.1 Structure of a Biological Neuron [64]

A mathematical model of a synthetic neuron node can be created using the same concept, as shown in figure 3.2. Data is received and conveyed through the input and output ports which represent the dendrites and axon terminals of the biologic neural cell. Only one input port and one output port are shown in the figure for the sake of simplicity, a bias term is also provided into the neuron node in order to compare random noises and any other unidentified factors that might have influenced the neuron cell's overall input. There is a function in the cell body which is called the activation function and as a result of the activation function, the cell body mimics the decision-making process of neurons. Output is the result of the processed information which is then sent to the next neuron in the chain.

Figure 3.2 Mathematical Abstraction of a Single Neuron[65]

By connecting more neurons, a single-layer perceptron can be produced in the appropriate way. Figure 3.3 shows that each pink circle in the diagram stands for an input

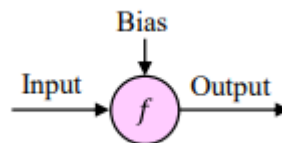neuron cell and each blue circle stands for an output neuron cell. The pink circles represent information sensory elements like dendrites, the axons which convey information are represented by the connection between the pink and blue circles and the axon terminals are shown by the blue circle. Each path's weight reflects the importance the cell assigns to that input path. The result in this illustration is the weighted sum of the inputs [65].
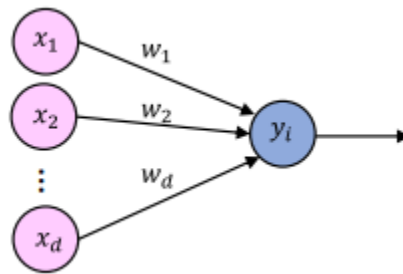
Figure 3.3 Structure of a Single-Layer Artificial Neural Network [65]

The mathematical equation of this model is:

$$\hat{y}_i = w_1 x_1 + w_2 x_2 + \ldots + w_d x_d \tag{3}$$

3.1 Activation Functions

There are different types of mathematical functions including sigmoid, arctangent, rectified linear unit, etc. which can be used as activation functions. A few well-known activation functions are briefly explained [66, 67].

3.1.1 Binary step function

One of the basic activation functions is the binary step function. It can act as an illustration of a trigger threshold that controls whether a neuron should activate or not. Figure 3.4 shows that the binary step function behaves much like a transistor the neuron is dormant if the input is below a particular threshold. The neuron gets triggered if the

input exceeds a particular threshold. However, the output is constant and has an unchanging range [67]. The mathematical expression of the binary step function is:

$$y=1 \quad \text{if } x>0 \tag{4}$$

$$y=0 \text{ if } x=<0$$
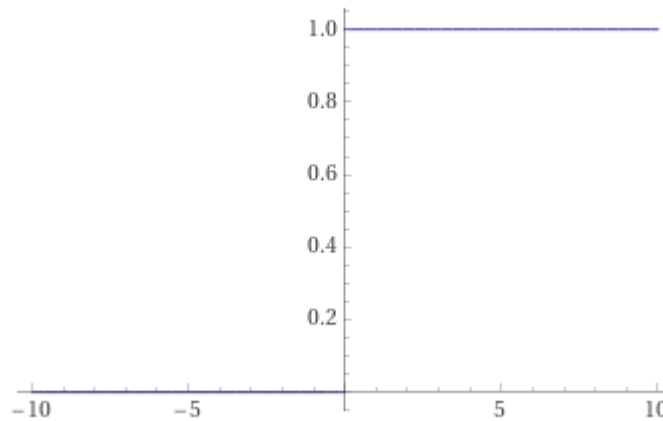
Figure 3.4 Binary Step Activation Function

3.1.2 Sigmoid function

The Sigmoid function is extensively employed as the activation function in many neural network projects. The Sigmoidal function is both nonlinear and steady. As seen in figure 3.5 it has a restricted output range between 0 and 1 and because of this feature, it is a strong choice for probability estimation [67]. Additionally the bell-shaped curve of its first -order derivative is similar to the normal distribution curve. It has various statistical merits over other activation functions as a result of this characteristic. The mathematical expression of the Sigmoid function is written below:

$$y = 1/(1+e^{-x}) \tag{5}$$
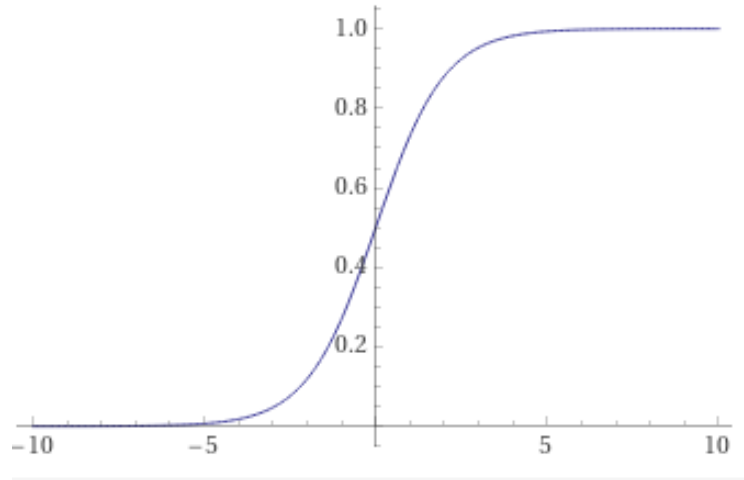
Figure 3.5 Sigmoid Function

3.1.3 Tangent hyperbolic function

Figure 3.6 represents the tangent hyperbolic activation functionwhich maps the input to the range (-1 , 1) [67]. When x is far from 0 it represents a steady increase and when x is close to 0 it switches to a fast growth stage. All x ranges are symmetric for a tangent hyperbolic function. Tangent's hyperbolic mathematical expression is:

$$y = \tanh(x) \tag{6}$$
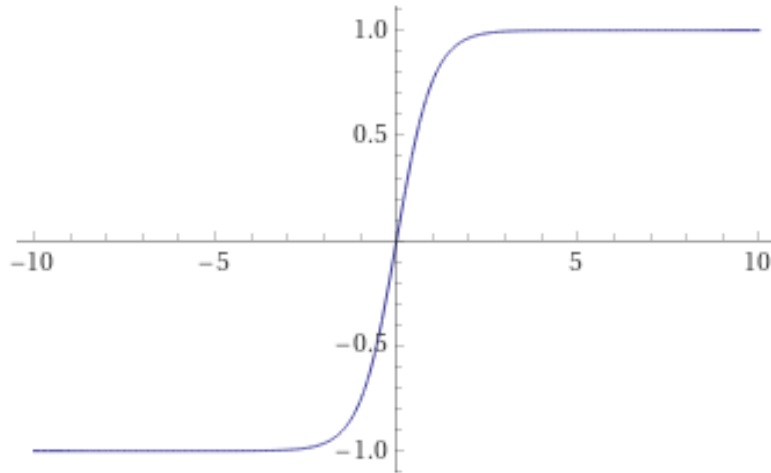
Figure 3.6 Tangent Hyperbolic Equation

3.1.4 The rectified linear unit function

Rectified linear unit function (ReLU) is a common non-linear activation function, particularly for deep learning projects. As demonstrated in figure 3.7 the function only responds to a specific range of inputs. If the input is negative, the output remains 0 and when the input is positive, the output is equal to the input value. Due to this feature, it can be used as a gate in neural networks to block unnecessary paths without physically altering the network architecture [67].

$$Y= \max (0, x) \qquad (7)$$
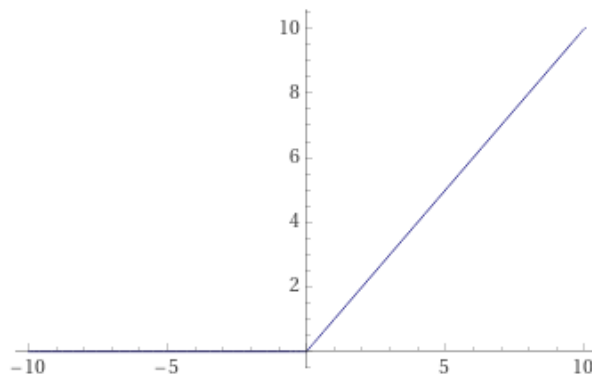
Figure 3.7 Rectified Linear Unit Function

3.2 Recurrent Neural Network (RNN)

Recurrent cell in RNN receives their output or permit connections between neurons in different layers [68]. Consequently, consecutive data can be recorded. There are several distinct varieties of RNNs based on various activation functions and link modalities such as long short-term memories and gated recurrent units. RNNs typically need more training time because the neuron's input value may depend on the number of neurons in the lower layers. In a real-world application, RNN is frequently used in statistics, speech recognition, and mobility pattern prediction. This study used one hidden layer containing 50 units and the optimization is carried out by ADAM optimizer [69]. The training was carried out on the google colab platform. Figure 3.8 shows the architecture of Recurrent neural networks. Neurons in the hidden layer receive their previous timestep output as the current time step input. The output of each timestep will be used as the input for the next time steps. the inner architecture of neurons in LSTM and GRU models is discussed in the next section.
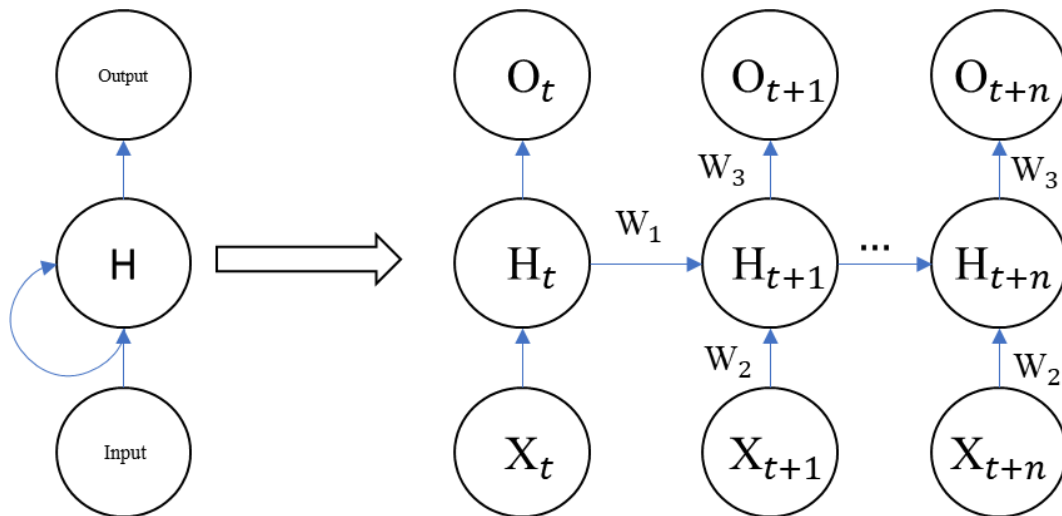
Figure 3.8 Schematic Diagram of Recurrent Neural Network [68]

3.3 LSTM

A type of recurrent neural network is called Long Short-Term Memory (LSTM) network. LSTM could master order dependency in sequence prediction problems. The RNN uses the outputs of the previous time steps as input to the next time step.The LSTM was developed by Hochreiter & Schmidhuber . By definition, the LSTM may hold data for a very long time [70]. It is employed in the analysis, forecasting, and classification of time-series data. LSTM includes feedback connections as opposed to typical feed-forward neural networks [71]. Along with managing individual data points, it can also handle whole data streams. Unsegmented, connected handwriting identification and speech recognition are two applications of LSTM. As seen in figure 3.9, the LSTM is composed of three sections, each of which has a distinct purpose.
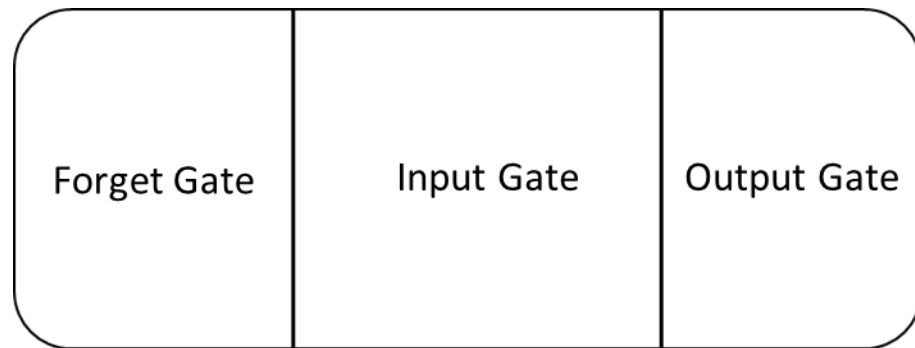
Figure 3.9 LSTM Cell Architecture

The forget section determines whether the data from the preceding time step has to be preserved or can be ignored. The cell attempts to learn new knowledge from the input to this cell in the input section. The cell finally transmits the revised data from the current time step to the next time step in the output section. LSTM cell sections are called gates. The Forget gate, Input gate, and Output gate are the names of the gates, respectively.

The LSTM also includes a hidden state, where H(t-1) stands for the hidden state of the previous timestep and H_t for the current timestep. Additionally, LSTMs contain a cell state. Cell state is denoted by C(t-1) and C(t), which stand for the prior and current cell state timesteps, respectively. The cell state is responsible for keeping data from earlier times inside the LSTM cell. The forget gate and input gate modify the cell state. The hidden state is the output of the LSTM cell. Figure 3.10 shows the cell state and hidden state flow in the LSTM cell. In this case, the cell state is referred to the long-term memory and the hidden state is the short-term memory [70].
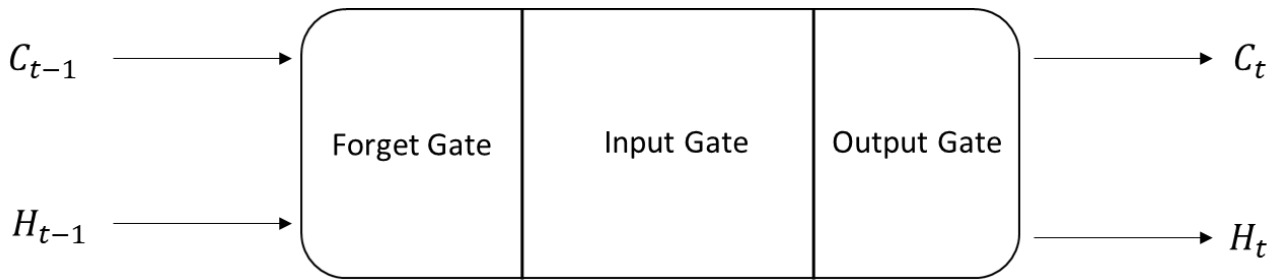
Figure 3.10 LSTM Information Flow

3.3.1 Forget Gate

The first step in an LSTM network cell is to decide whether to preserve or discard the data from the preceding timestep [70]. The forget gate formula is shown below.

$$F_t = \sigma(W_f.[X_t * h_{t-1}] + b_f) \tag{8}$$

X_t: current timestep input

U_f: input weight

h_{t-1}: the previous timestep hidden state

W_f: hidden state weight

A Sigmoid function is then added to it later as a result F_t will be a number between 0 and 1. As seen below this F_t is then multiplied by the cell state of the prior timestamp.

$$C_{t-1} * F_t = 0 \dots \text{if } F_t = 0 \text{ (forget everything)}$$

$$C_{t-1} * F_t = C_{t-1} \dots \text{I}$$

$$\text{if } F_t = 1$$

(Forget nothing)

The network will forget everything if F_t is set to 0, but nothing if F_t is set to 1.

3.3.2 Input Gate

Input gates are employed to evaluate the significance of the fresh information carried by the input. The input gate selects the relevant data which can be added from the current step [70]. The equation of the input gate is shown below:

$$i_t = \sigma(X_t * U_i + H_{t-1} * W_i) \tag{9}$$

X_t: current timestep Input

U_i: input weight

H_{t-1}: the previous timestep hidden state

W_i: hidden state weight

The sigmoid function is applied to the results. The final value of the input gate is a value between 0 and 1 at timestep t.

3.3.3 Output Gate

$$N_t = tanh(X_t * U_c + H_{t-1} * W_c) \tag{10}$$

A hidden state at timestep t-1 and input x at timestep t is now required in order to send the new information to the cell state. tanh is the activation function. The tanh function regulates new data and puts them in a range of -1 to 1. If the value of N is negative, the information is subtracted from the cell state, and if it is positive, the information is added to the cell state at the current timestep [70]. However, N_t will not be added directly to the cell state. The revised equation is seen below:

$$C_t = F_t * C_{t-1} + i_t * N_t \text{ (Updating cell state)} \tag{11}$$

In this case C_{t-1} represents the cell state at the previous time step, and the other variables are those we previously computed. The output gate's equation, which is quite identical to the formulas for the first two gates, is shown below:

$$O_t = \sigma(X_t * U_o + H_{t-1} * W_o) \tag{12}$$

Due to the effect of the Sigmoid function, the output will have a value between 0 and 1. To calculate the current hidden state, we will now utilize O_t and tanh of the updated cell state as displayed below:

$$H_t = O_t * \tanh(C_t) \tag{13}$$

It turns out that the hidden state relies on both the present output and long-term memory (C_t) [70]. Figure 3-11 shows the structure of LSTM.
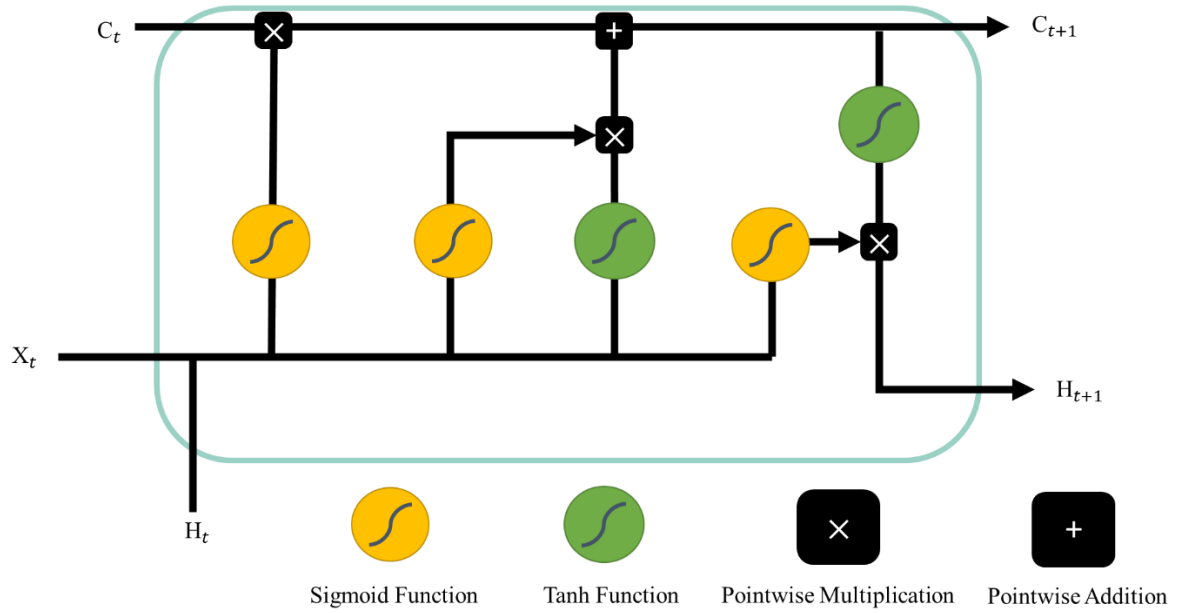
Figure 3.11 LSTM Structure[64]

The LSTM cell contains 3 sigmoid functions and 2 tanh functions.

3.4 GRU

GRU is very similar to Long Short-Term Memory. Both use gates to control the flow of information. GRU in contrast with LSTM does not have a separate cell (C_t). It only has a hidden state (H_t) [72, 73]. Figure 3.12 shows the architecture of the GRU cell.
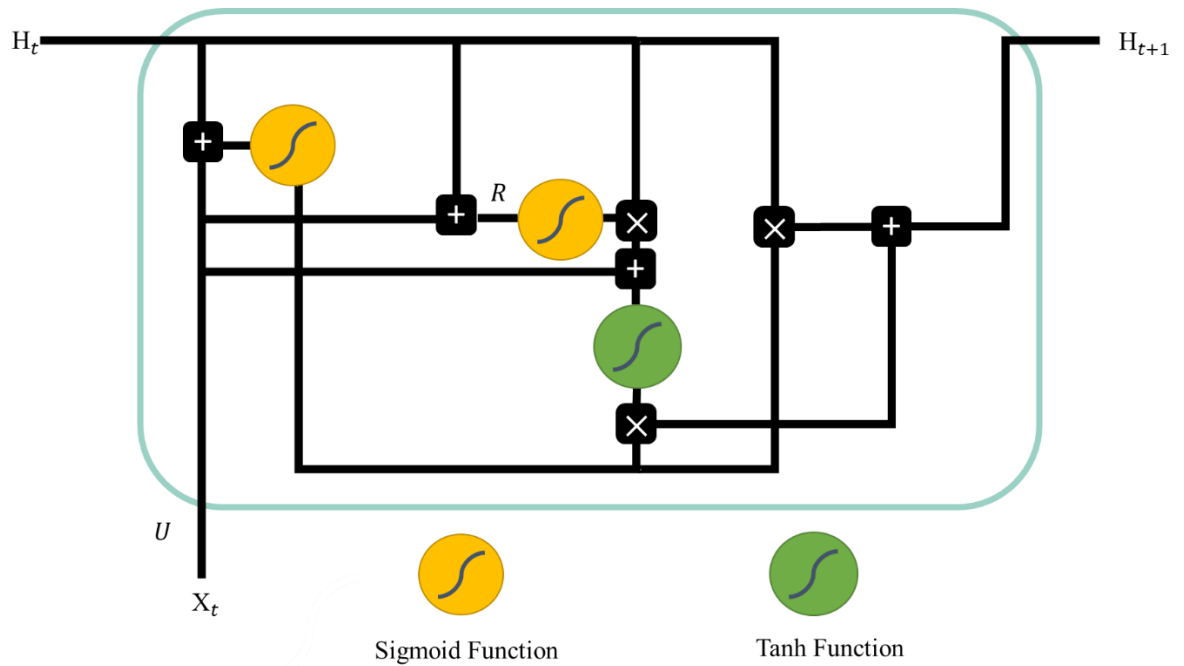
Figure 3.12 GRU Structure

3.4.1 The Architecture Of The Gated Recurrent Unit

Here we have a GRU cell that resembles an LSTM or RNN cell more or less. The GRU cell gives the new hidden state, which is passed on to following cells, after receiving the previous hidden state and the current inputs. In contrast with LSTM, GRU has only two gates. The GRU gates are reset gate and update gate [73].

3.4.2 Reset Gate (Short term memory)

The network's short-term memory is handled by the reset gate. The reset gate specifies the amount of information from the past that should be forgotten[73]. The reset gate's equation is given below:

$$r_t = \sigma(X_t * U_r + H_{t-1} * W_r) \tag{14}$$

44

The r_t will have a value between 0 and 1 as a result of the Sigmoid function. The weight matrices for the reset gate are U_r and W_r [73].

3.4.3 Update Gate (Long Term memory)

Update gate filters previous data and allows some of it to pass along to the future[73]. The equation of the update gate for long-term memory is:

$$u_t = \sigma(X_t * U_u + H_{t-1} * W_u) \tag{15}$$

3.4.4 How GRU Works

Two steps are taken to obtain the hidden state (H_t) In GRU. The first step is the creation of the candidate's hidden state.

3.4.5 Candidate Hidden State

$$\widehat{H}_t = tanh(X_t * U_g + (r_t°H_{t-1}) * W_c \tag{16}$$

It receives the preceding timestep's input and hidden state, t-1, and multiplies those values by the reset gate output, r_t. Later passed this whole data to the tanh function, and the outcome value is the candidate's hidden state [72, 73]. The most crucial aspect of this equation is how we are able to regulate how much impact the previous hidden state can have on the candidate state by adjusting the reset gate's value. The whole information from the previous hidden state H_{t-1} is taken into account if the value of r_t equals 1. The information from the preceding hidden state is completely ignored if the value of r_t is 0.

3.4.6 Hidden State

Once we have the candidate state, it is utilized to create the current hidden state. An update gate is used in determining the hidden state. Unlike LSTM, GRU uses only one gate to regulate previous and current data entering from the current timestep [39, 72, 73].

$$H_t = u_t{}^\circ H_{t-1} + (1 - u_t)^\circ \widehat{H}_t \qquad (17)$$

Assuming that u_t is close to 0 then the first term which is shown by the red color in the equation will vanish which means that a little information from the previous hidden state will be carried over to the current hidden state. However, if u nearly approach one, which basically indicates that the candidate state will be the only source of information for the hidden state at this timestep.

$$H_t = u_t{}^\circ H_{t-1} + (1 - u_t)^\circ \widehat{H}_t \qquad (18)$$

If the value of second term or $1 - u_t$ which is shown by red color, has become entirely 0 then the information from the hidden state at the previous timestep t-1, will be the only factor that influences the first term, or the present hidden state.

$$H_t = u_t{}^\circ H_{t-1} + (1 - u_t)^\circ \widehat{H}_t \qquad (19)$$

As a result, we may infer that the value of u_t , which ranges from 0 to 1, is quite important in this formula. The training process steps in the recurrent neural networks are briefly described below. The network is initialized by assigning the number of units to the layers, creating the layering structure, defining the activation functions, and setting the number of iterations. The training process is started by inputting the corresponding data at time to the model. First, RNN units in the layers compute gate results and pass the final output through the output gate, having the outputs, the difference between the actual

and predicted value is calculated and the weights of the models are adjusted on a continuous basis of error calculation. Finally, the corresponding data at time t+1 is fed to the model and the above steps are repeated. This training process continues till the end condition which is obtaining the constant error met.

3.5 Root Mean Square Error

The root means square error formula for checking the accuracy of models is shown below. N is the number of parameters, x_i is the estimation and $\hat{x}_i$ is the actual data [74].

$$RMSE = \sqrt{\frac{\sum_{i=1}^{N}(x_i - \hat{x}_i)^2}{N}}$$

(20)

3.6 Correlation Between Parameters

The Least Absolute Shrinkage and Selection Operator (LASSO) is a well know statistical regularization method for feature selection [75, 76]. For a more accurate forecast, lasso regression is preferred over regression techniques. The Lasso model uses shrinkage and shrink data values to central points. This method is mostly used for models with high correlations or model selections such as parameter selection. Regularization adds a penalty term to the fitted line on the training data and decreases the variance between the test data and the fitted line. Regularization reduces the effect of predictor parameters over output by compressing their coefficients [75, 76]. The cost function mathematical equation for lasso regression is

Residual Sum of Squares + λ * (Sum of the absolute value of the magnitude of coefficients)

$$\sum_{i=1}^{n} (y_i - \sum_{j} x_{ij}\beta_j)^2 + \lambda \sum_{j=1}^{p} |\beta_j| \qquad (21)$$

- λ (lambda) is the amount of penalty(shrinkage).
- $\lambda = 0$ includes all features and it is equal to the normal regression
- $\lambda = \infty$ excludes all features and all feature coefficients are zero.
- β_j is the coefficient of parameters.

This model fits a line to the output by adding a penalty (λ) term. The penalty term eliminates unnecessary parameters by reducing the coefficients. A high penalty excludes the effects of all features, and no penalty will include all parameters in the regression. The penalty term (Lambda) is determined by cross-validation. In cross-validation, the dataset is divided into multiple divisions and one of the divisions is used for the test while the other divisions are used for training. Training divisions are used to fit data with different penalties and the fitted line is tested with test data. These divisions change their roles iteratively and the lambda with the lowest error will be calculated in each of these setups. The penalty with the lowest cost function will be found. The suitable penalty will be used in the cost function and the sum of coefficients will decrease to find the lowest error point while decreasing coefficients. The coefficients which tend to be zero indicate the non-important parameters. Figure 3.13 shows important parameters for the state of charge prediction. All 16 features used in the models are shown in the figure 3.13.
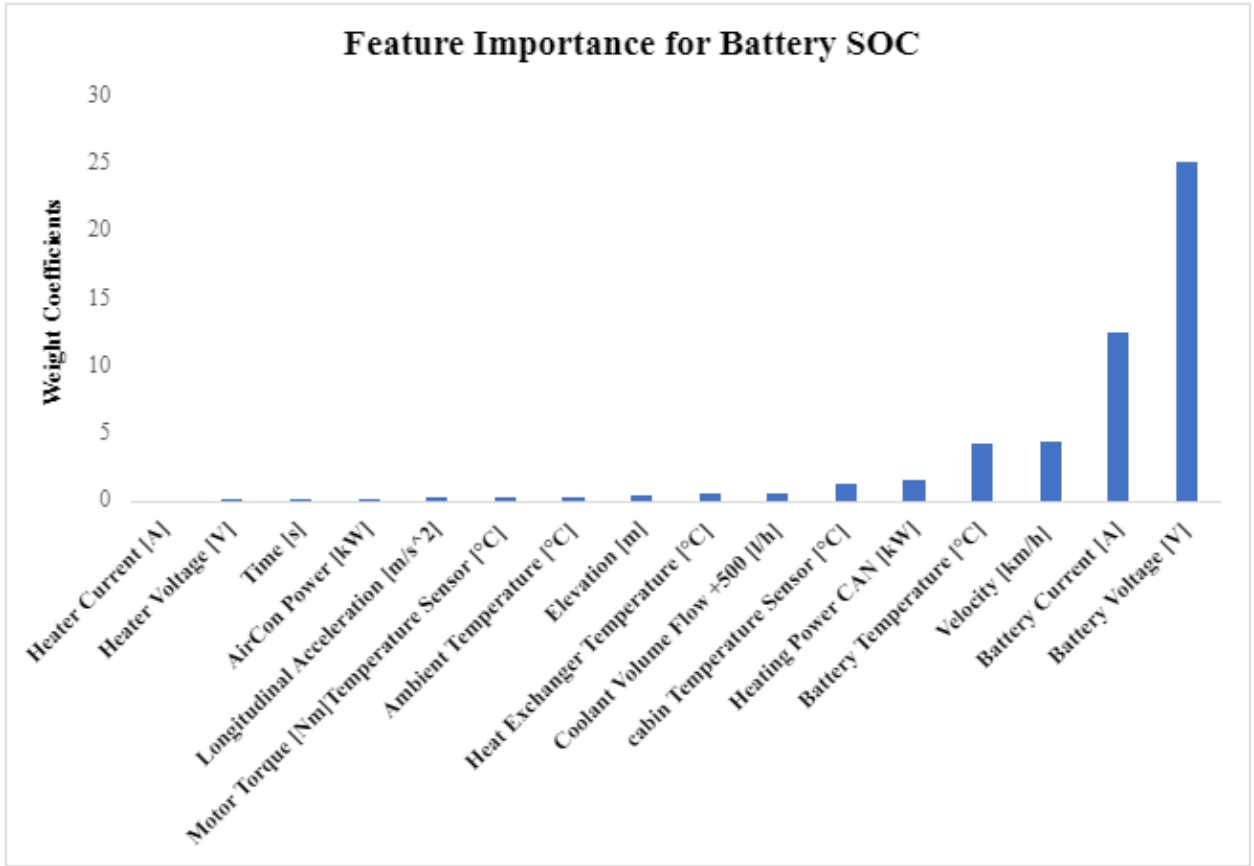
Figure 3.13 Feature Importance for Battery SOC

The Lasso model eliminated about 10 features by reducing their coefficients. Battery voltage and current, Velocity, Battery temperature, and heating power are the most important parameters for estimating the Battery state of charge. Parameters such as heater current, voltage, and air conditioning power have a weak correlation with the battery SOC. In environmental features, Elevation has the highest correlation with the battery state of charge. Figure 3.14 shows the important parameters for Battery temperature prediction. All 16 features included in the training are shown in the figure.
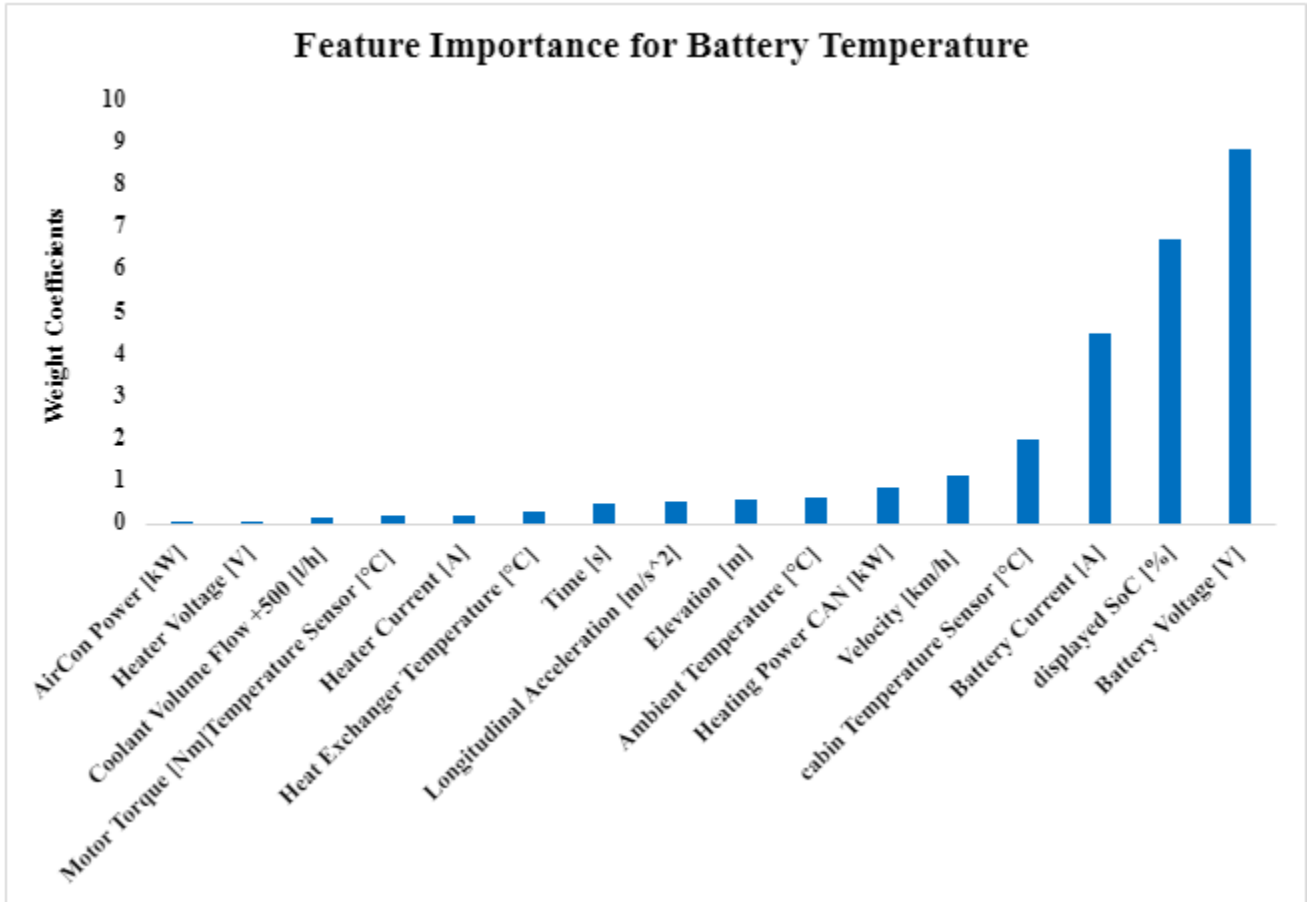
Figure 3.14 Feature Importance for Battery Temperature

In contrast with the Lasso technique employed for battery SOC, Lasso couldn't reduce the coefficients of parameters in battery temperature correlation computation. Battery voltage and current, velocity, battery state of charge, and cabin temperature are the most important parameters for estimating battery temperature. The battery voltage has the highest correlation with the battery temperature. In terms of environmental factors, the correlation between ambient temperature and battery temperature is the strongest.

CHAPTER 4

RESULT AND DISCUSSION

4.1 Recuperation & Heating Share Response

Figure 4.1 shows the heating share based on the ambient temperature at the beginning of each drive cycle. Each drive cycle is represented by a point in the figure. Moreover, all winter driving trips are included in this analysis. There is a negative correlation between ambient temperature and heating share. When the ambient temperature drops, the heating energy share will be increased.
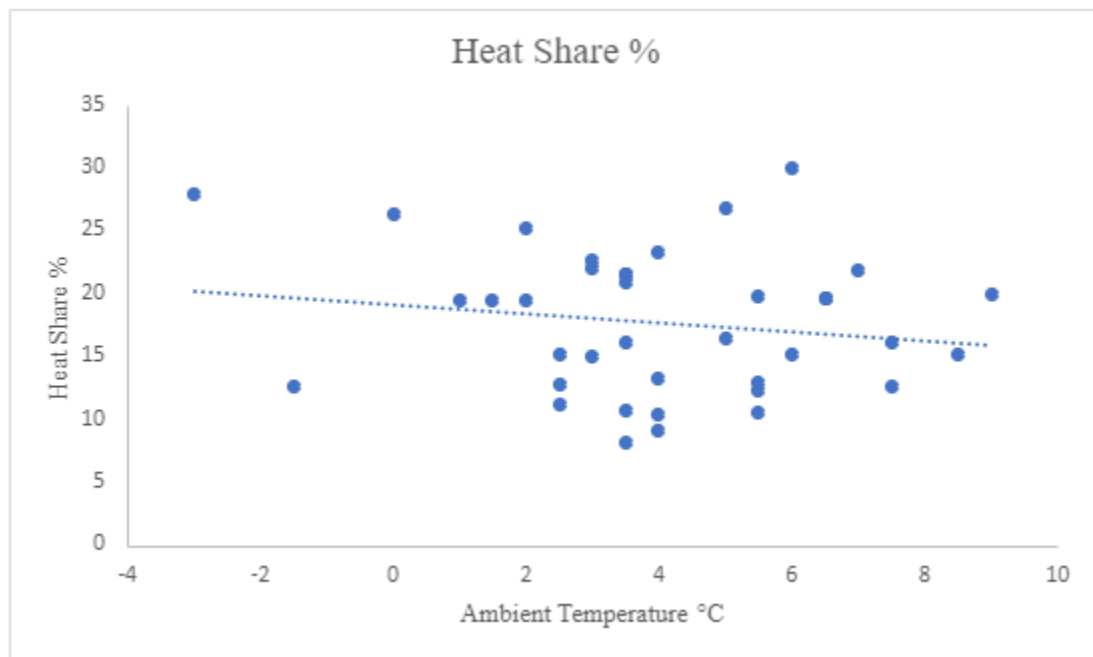
Figure 4.1 Heat Share of Drive Cycles in Different Ambient Temperatures

Every 3 degrees of ambient temperature drop results in a 1% increase in the heating energy share. Based on the figure, 20% of the total energy in a drive cycle consumption is consumed by the heating system at -3 °C. Figure 4.2 compares the energy recovered during a trip to the energy needed to fulfill the traction energy requirements for all winter

trips in the database. Instead of total energy usage which includes heating energy, the traction energy demand is taken into account. This is an isolated approach to determining the influence of temperature on recuperation with respect to the vehicle's energy consumption.
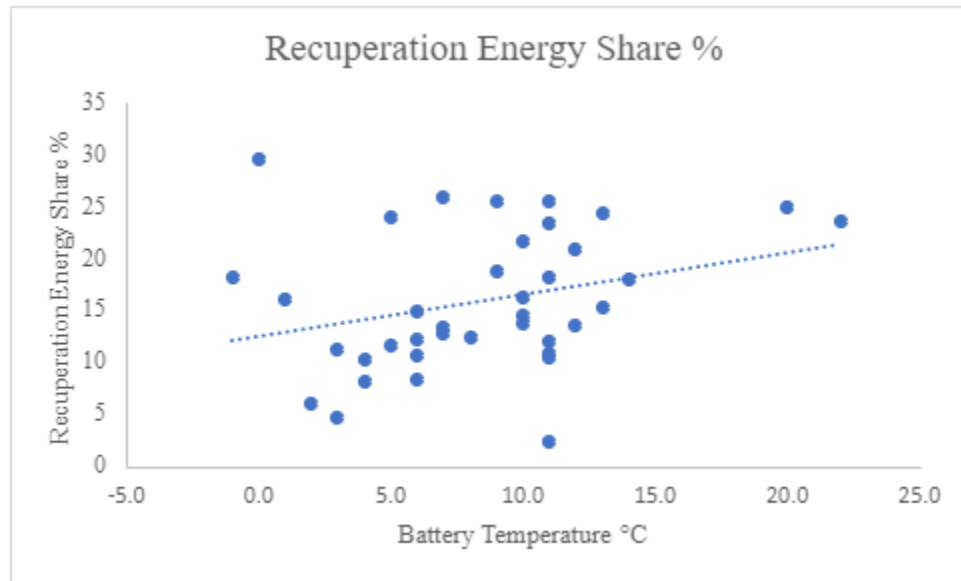
Figure 4.2 Recuperation Energy Share%

Based on the figure 4-2, Recuperation energy share and battery temperature have a positive correlation. Recuperation energy will decrease as the battery temperature drops. On average each 5-degree increase in battery temperature will lead to a 2% increase in the recuperation energy share.

4.2 Vehicle Data Distribution

Battery temperature variations, ambient temperature variations, voltage, SOC, Heat exchanger temperature, and cabin temperature data points densities are included in figure 4.3. Data points in all winter trips are summarized. The range of winter ambient temperature range is provided along with the vehicle heating system data distribution.

This chart will not only provide details about the distribution of data points but will describe the behavior of the heating system.
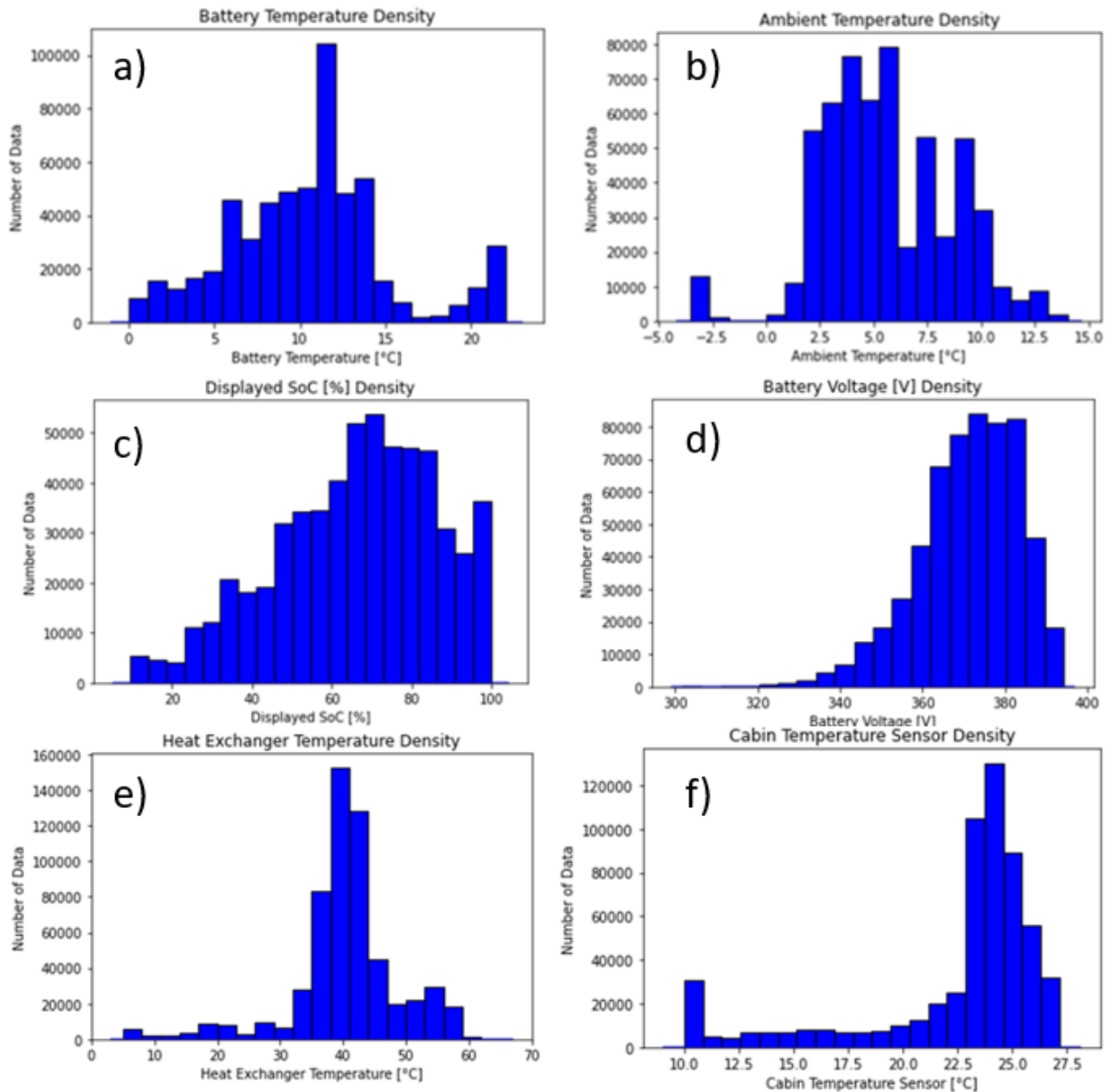
Figure 4.3 Distribution of Data in All Winter Trips; A) Battery Temperature Data Distribution, B) Ambient Temperature Data Distribution, C) Displayed SOC Data Distribution, D) Battery Voltage Data Distribution, D) Heat Exchanger Temperature Data Distribution, F) Cabin Temperature Data Distribution

Based on the figure, heat exchanger and cabin temperatures are correlated. The coolant warms up fast and heats the cabin, this behavior changes the density of data points on the

upper limits of the cabin and heat exchanger temperatures. The battery voltage and battery SOC are correlated, the voltage of the battery varies from 320 to 400 V based on the Figure. Part e shows that the heat exchanger outlet is mostly between 30 – 50 C. Battery, cabin, and ambient temperatures are correlated as they influence the battery package temperature. Moreover, The battery temperature distribution range is mostly between 5 - 15 C which is not an efficient and safe battery temperature to operate.

4.3 Battery SOC Prediction

The unavoidable variations in SOC and battery temperature data are estimated with the help of machine learning. This precise pattern recognition is one of the strength points of machine learning methods. The data from the previous timesteps are used by the LSTM and GRU models to anticipate SOC, and battery temperature for the upcoming timesteps, enabling an accurate SOC and battery temperature forecast to improve electric vehicle control schemes and evaluate the effects of additional equipment. The models used Time [s],Velocity [km/h],Elevation [m],Motor Torque [Nm],Longitudinal Acceleration [m/s^2],Battery Voltage [V],Battery Current [A],Battery Temperature [°C],Heating Power CAN [kW],Air conditioner Power [kW],Heater Voltage [V],Heater Current [A],Ambient Temperature [°C],Coolant Volume Flow +500 [l/h],Heat Exchanger Temperature [°C] and Cabin Temperature Sensor [°C] data as inputs of the model. LSTM and GRU models have been trained with about 80% of data and 20% for validation of models. 32 drive cycles were used for training and 6 drive cycles were used for validation out of 38 datasets. In most of the driving cycle charts, LSTM outperforms GRU. Both models are similar to each other since they have pretty much similar architecture. LSTM has one gate more than GRU which allows it to process data more,

but it is more complex. However, GRU is fast compared to LSTM, and it has less complexity. Figure 4.4 shows LSTM, GRU estimations, and actual SOC of the electric vehicle data for drive cycles 33 to 38.
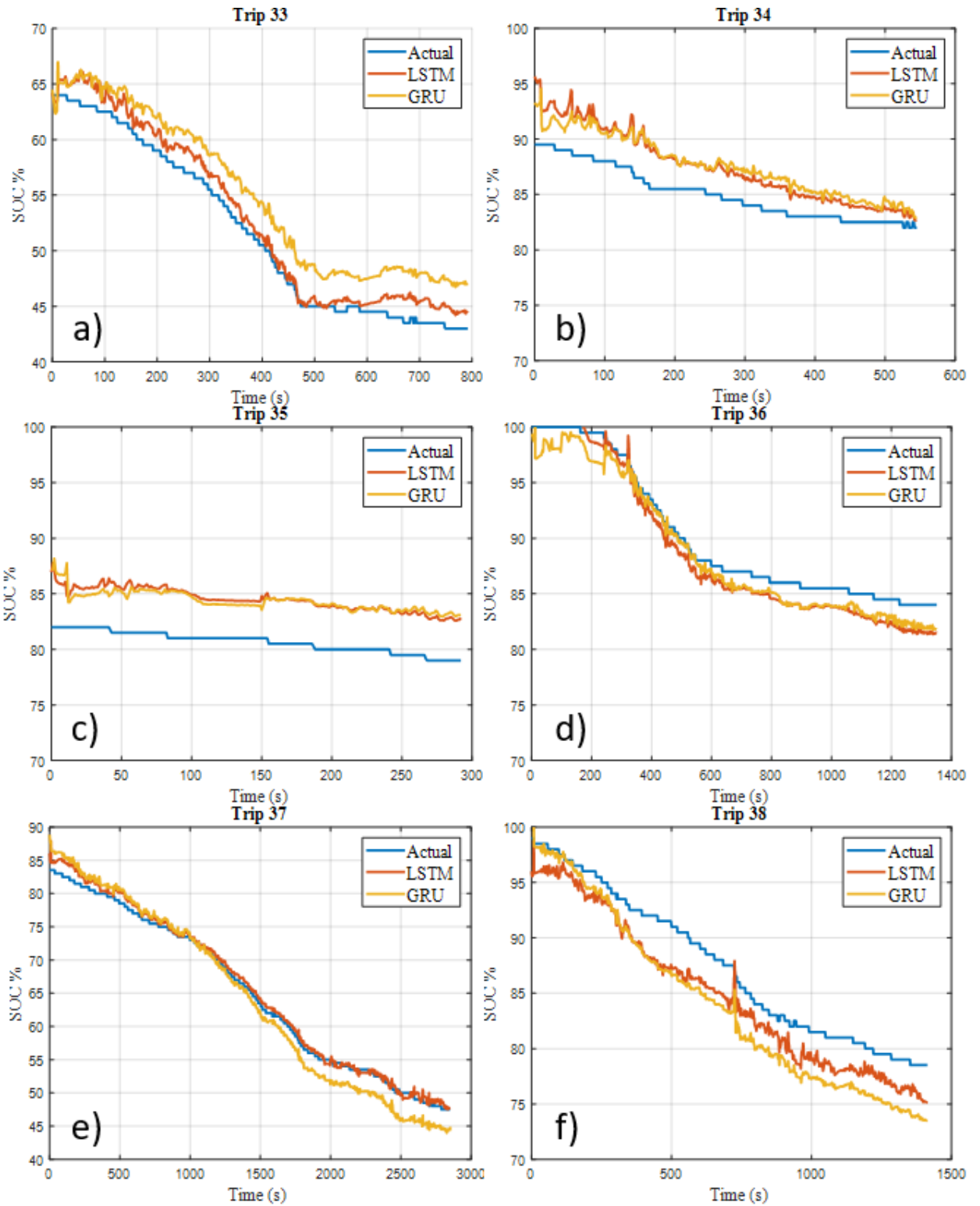
Figure 4.4 LSTM, GRU   SOC Estimations; A) Trip 33 Results, B) Trip 34 Results, C) Trip 35 Results, D) Trip 36 Results, E) Trip 37 Results, F) Trip 38 Results,

LSTM converges to the actual value of SOC, faster and it has less noise compared to GRU. LSTM has outperformed GRU on all the trips. GRU estimations are noisier than LSTM results. This noise reduction is the result of the additional activation functions in the LSTM, such as the sigmoid and tanh. In addition to preventing linearity in LSTM cell results, these functions also filter out unnecessary information. This extra data filtration might be the reason for noise reduction.

4.4 Battery Temperature Prediction

The battery pack of the BMW i3 is mostly in a non-efficient temperature range. Same as SOC, 80% or 32 drive cycles are used for training and 20% are used for validation of battery temperature estimation models. The models used Time [s],Velocity [km/h],Elevation [m],Motor Torque [Nm],Longitudinal Acceleration [m/s^2],Battery Voltage [V],Battery Current [A], displayed SOC [%],Heating Power CAN [kW],Air conditioner Power [kW],Heater Voltage [V],Heater Current [A],Ambient Temperature [°C],Coolant Volume Flow +500 [l/h],Heat Exchanger Temperature [°C] and Cabin Temperature Sensor [°C] data as inputs of the model. Since the battery in the battery pack temperature is influenced by lots of factors such as current variation, velocity, heating /cooling effects of air conditioning, etc., estimations fluctuate. Irreversible heat generation is influenced by the internal resistance of the battery and current, these factors are influenced by ambient temperature, energy consumption, and heating/cooling system. Reversible heat generation results in entropy change and it changes by temperature. Furthermore, Energy transfer through convection is majorly influenced by the ambient

temperature and velocity. Instead of using the theoretical approach for calculating battery temperature; machine learning models have been developed in order to identify patterns of temperature estimation. Figure 4.5 shows the LSTM and GRU estimation and compares them with the actual battery temperature in different drive cycles. These estimations can be used to eliminate temperature sensors and increase battery pack space.
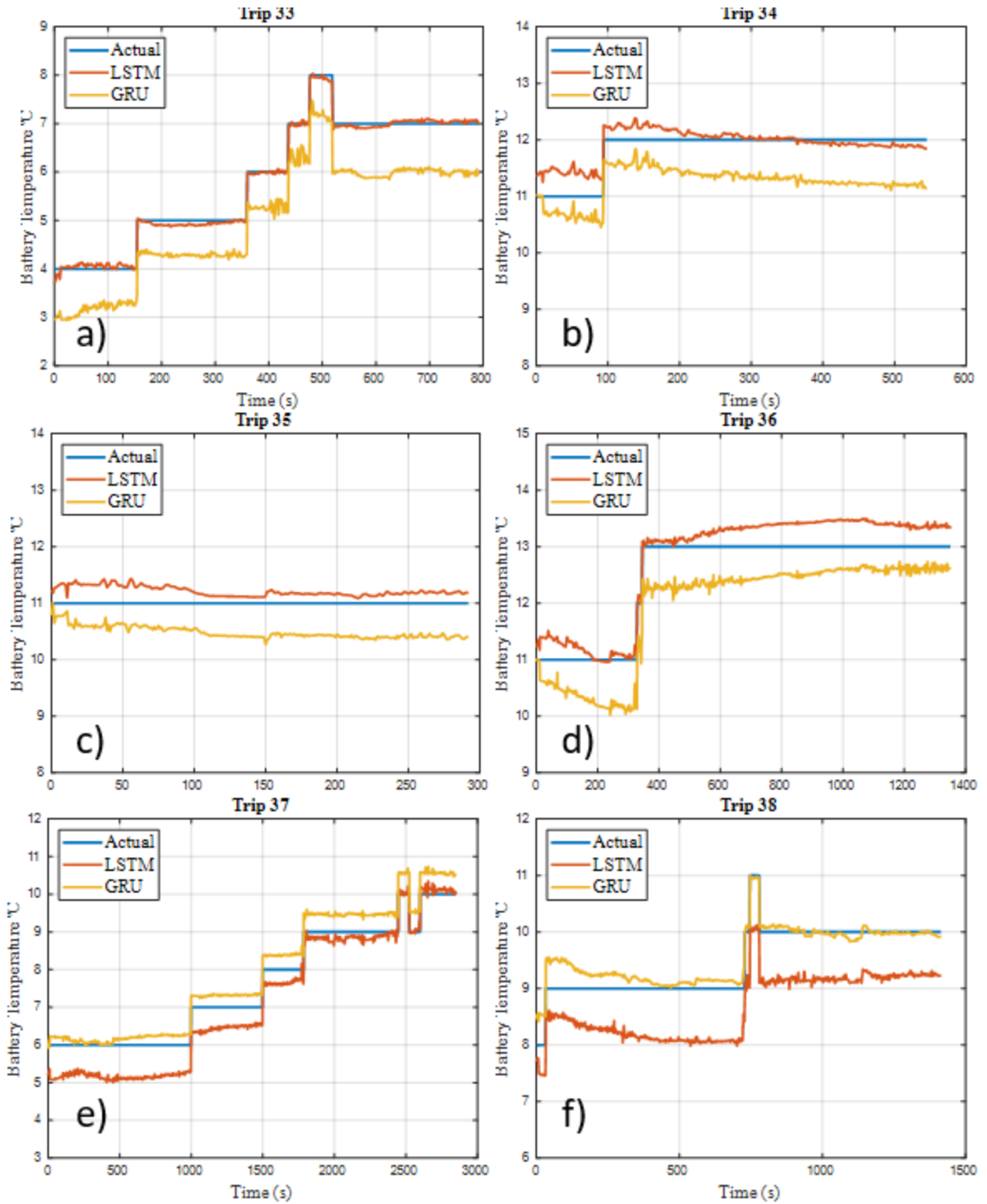
Figure 4.5 LSTM, GRU Battery Temperature Estimations A) Trip 33 Results, B) Trip 34 Results, C) Trip 35 Results, D) Trip 36 Results, E) Trip 37 Results, F) Trip 38 Results,

In all of the trips, LSTM had better convergence toward actual data. Based on the achieved results in trip 35, the estimation error of the GRU model worsened as time

passed, but the LSTM model got better. This result proves that complex datasets such as the dataset used in this study need more data processing gates. The LSTM handled the data processing better since it is more complicated and has an additional gate. The obtained results in trip 38, show that GRU model predictions are closer to the actual value and LSTM estimations have a bias which caused more error.

LSTM and GRU models are compared in terms of efficiency in estimating battery temperature and battery state of charge. The root means square error (RMSE) of each model is included to show the accuracy of each model. Table 4.1 shows the RMSE of each model in SOC and battery temperature estimations.

Table 4.1 RMSE Comparison Between LSTM and GRU

RMSE	Battery Temperature °C	State Of Charge %
LSTM	0.29 °C	2.23%
GRU	0.70 °C	2.52%

According to the table, LSTM is superior to the GRU in both states of charge and battery temperature estimation. This superiority is the result of having one extra gate compared to GRU, but the accuracy difference is not much in the state of charge estimations. So GRU might be a practical and better model for estimating the state of charge since it is less complex. Figure 4.6 shows the effect of training percentage on the RMSE. By increasing the training percentage, the error decreases. The error doesn't change a lot when at least 70 % of the data is used for the training.
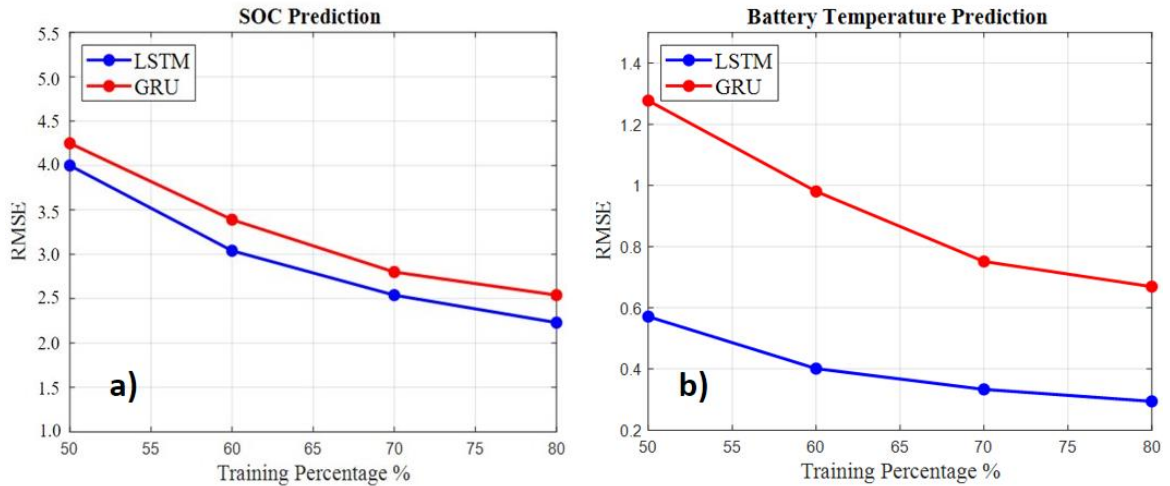
Figure 4.6 Training Percentage Variations and The Resulting RMSE; A) Training Data Percentage vs SOC B) Training Data Percentage vs Battery Temperature

In the correlation section of this study, important features for each of the estimations are shown. For battery temperature forecast the six most important features are battery voltage, battery state of charge, battery current, cabin temperature, velocity, and heating power. Battery voltage, battery current, velocity, battery temperature, heating power, and cabin temperature parameters are the important features for state of charge estimation. These features are used for estimations to determine the effect of the number of parameters on the performance of estimation models. Figure 4.7 shows the performance variation of models while trained with a different number of parameters.
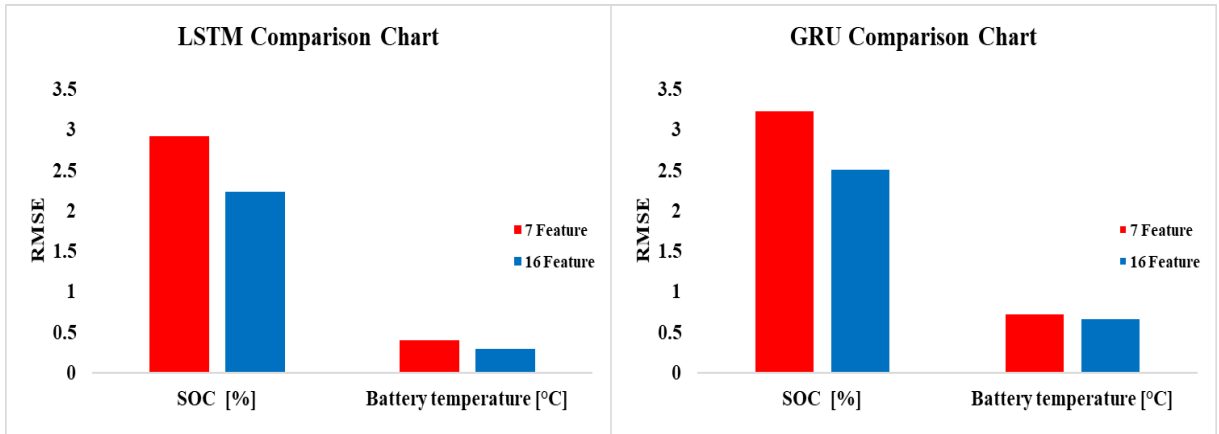
Figure 4.7 RMSE Comparison of 7 Feature and 16 Feature Models; A) LSTM Models Comparison, B) GRU Models Comparison

Based on the comparison chart, using 7 features doesn't have a strong effect on the performance of the battery temperature models. In the state of charge prediction, the RMSE difference between the 7-feature model and the 16-feature model is about 1%.

CHAPTER 5

CONCLUSION

The low driving range is one of the weak points of electric vehicles. Particularly, low temperatures have a significant negative effect on its range which is resulted from heating energy consumption. Moreover, in low temperatures, the regenerative braking system is not capable of generating a significant amount of energy due to an increase in impedance. This study covered the effects of low temperatures on heating energy demand. On average 20% of BMW i3 energy consumption is for heating at the ambient temperature of -3 °C. In addition, a detailed analysis of regenerative braking behavior was determined theoretically. On average each 5 degree increase in battery temperature will lead to a 2% increase in the recuperation energy share.

The second part of the study covered the machine learning approach to determine important parameters such as SOC and battery temperature. These parameters which are correlated with different parts of the electric vehicle have been estimated to prevent overcharge and discharge, thermal runaway, and cold damage to the battery. LSTM and GRU models have been compared in terms of estimation accuracy. In battery temperature estimation and SOC estimations, LSTM has achieved RMSE of 0.29 °C and 2.23% respectively. In battery temperature estimation and SOC estimations, GRU has achieved RMSE of 0.70 °C and 2.52% respectively. In both SOC and battery temperature estimation, LSTM was more accurate based on the root mean square error. The effect of train percentage over RMSE shows that using about 70 % of the data for training could be sufficient. Moreover, the effects of reducing the number of parameters on the model accuracy are determined. The battery temperature models using 7 features are performing

relatively well compared to the models using 16 features. But the error between 7 and 16 feature models in SOC estimation is high.

The results and the models of this study could be further developed and implemented on the BMW i3 electronics. Future research can focus on control strategies based on these machine learning models in order to increase electric vehicles driving range. These control strategies can work on the thermal sensor replacements in battery, charging, and discharging control with respect to the battery temperature and state of charge forecast using different parameters.

REFERENCES

1.   López-Claros, A., A.L. Dahl, and M. Groff, *Global governance and the emergence of global institutions for the 21st century*. 2020: Cambridge University Press.
2.   Masson-Delmotte, V., et al., *Global warming of 1.5 C.* An IPCC Special Report on the impacts of global warming of, 2018. **1**(5).
3.   Delphi, T.M., *Worldwide Emissions Standards-Passenger Cars and Light Duty.* 2017.
4.   Bibra, E.M., et al., *Global EV Outlook 2021: Accelerating Ambitions Despite the Pandemic.* 2021.
5.   Hathaway, Z., et al., *A Utility Roadmap for Expanding Customer Adoption of Electric Vehicles.* World Electric Vehicle Journal, 2021. **12**(2): p. 81.
6.   Bonges III, H.A. and A.C. Lusk, *Addressing electric vehicle (EV) sales and range anxiety through parking layout, policy and regulation.* Transportation Research Part A: Policy and Practice, 2016. **83**: p. 63-73.
7.   Adhikari, M., et al., *Identification and analysis of barriers against electric vehicle use.* Sustainability, 2020. **12**(12): p. 4850.
8.   She, Z.-Y., et al., *What are the barriers to widespread adoption of battery electric vehicles? A survey of public perception in Tianjin, China.* Transport Policy, 2017. **56**: p. 29-40.
9.   Yuksel, T. and J.J. Michalek, *Effects of regional temperature on electric vehicle efficiency, range, and emissions in the United States.* Environmental science & technology, 2015. **49**(6): p. 3974-3980.
10.   Iora, P. and L. Tribioli, *Effect of ambient temperature on electric vehicles' energy consumption and range: Model definition and sensitivity analysis based on nissan leaf data.* World Electric Vehicle Journal, 2019. **10**(1): p. 2.
11.   Ding, Y., et al., *Automotive Li-ion batteries: current status and future perspectives.* Electrochemical Energy Reviews, 2019. **2**(1): p. 1-28.
12.   Ayartürk, H., et al., *New heating system development working with waste heat for electric vehicles.* Transportation Research Procedia, 2016. **14**: p. 1080-1086.
13.   Dvorak, D., D. Basciotti, and I. Gellai, *Demand-Based Control Design for Efficient Heat Pump Operation of Electric Vehicles.* Energies, 2020. **13**(20): p. 5440.
14.   Horrein, L., et al., *Impact of heating system on the range of an electric vehicle.* IEEE transactions on Vehicular Technology, 2016. **66**(6): p. 4668-4677.
15.   Reyes, J.R.M.D., R.V. Parsons, and R. Hoemsen, *Winter happens: The effect of ambient temperature on the travel range of electric vehicles.* IEEE Transactions on Vehicular Technology, 2016. **65**(6): p. 4016-4022.
16.   Michaelides, E.E., *Thermodynamics and energy usage of electric vehicles.* Energy Conversion and Management, 2020. **203**: p. 112246.
17.   Taggart, J. *Ambient temperature impacts on real-world electric vehicle efficiency & range.* in *2017 IEEE Transportation Electrification Conference and Expo (ITEC).* 2017. IEEE.

18. Habedank, J.B., J. Kriegler, and M.F. Zaeh, *Enhanced fast charging and reduced lithium-plating by laser-structured anodes for lithium-ion batteries.* Journal of The Electrochemical SOCiety, 2019. **166**(16): p. A3940.

19. Nagasubramanian, G., *Electrical characteristics of 18650 Li-ion cells at low temperatures.* Journal of applied electrochemistry, 2001. **31**(1): p. 99-104.

20. Aris, A.M. and B. Shabani, *An experimental study of a lithium ion cell operation at low temperature conditions.* Energy Procedia, 2017. **110**: p. 128-135.

21. Steinstraeter, M., et al., *Range extension via electrothermal recuperation.* World Electric Vehicle Journal, 2020. **11**(2): p. 41.

22. Tomaszewska, A., et al., *Lithium-ion battery fast charging: A review.* ETransportation, 2019. **1**: p. 100011.

23. Garniwa, I., et al. *Analysis of the effect of the motor temperature to brushless direct current motor performance on KARLING electric vehicle*. in *Journal of Physics: Conference Series*. 2019. IOP Publishing.

24. El Naqa, I. and M.J. Murphy, *What is machine learning?*, in *machine learning in radiation oncology*. 2015, Springer. p. 3-11.

25. Steinstraeter, M., T. Heinrich, and M. Lienkamp, *Effect of Low Temperature on Electric Vehicle Range.* World Electric Vehicle Journal, 2021. **12**(3): p. 115.

26. Goodfellow, I., Y. Bengio, and A. Courville, *Deep learning*. 2016: MIT press.

27. Chung, J., et al., *Empirical evaluation of gated recurrent neural networks on sequence modeling.* arXiv preprint arXiv:1412.3555, 2014.

28. Crocioni, G., et al., *Li-ion batteries parameter estimation with tiny neural networks embedded on intelligent iot microcontrollers.* IEEE Access, 2020. **8**: p. 122135-122146.

29. Gers, F., *Long Short-Term Memory in Recurrent Neural Networks, Ph. D. Thesis.* University of Hanover, Hanover, 2001.

30. Hochreiter, S. and J. Schmidhuber, *Long short-term memory.* Neural computation, 1997. **9**(8): p. 1735-1780.

31. Cho, K., et al., *On the properties of neural machine translation: Encoder-decoder approaches.* arXiv preprint arXiv:1409.1259, 2014.

32. Sak, H., A.W. Senior, and F. Beaufays, *Long short-term memory recurrent neural network architectures for large scale acoustic modeling.* 2014.

33. Malhotra, P., et al., *LSTM-based encoder-decoder for multi-sensor anomaly detection.* arXiv preprint arXiv:1607.00148, 2016.

34. Wang, G., et al., *A short-term voltage stability online prediction method based on graph convolutional networks and long short-term memory networks.* International Journal of Electrical Power & Energy Systems, 2021. **127**: p. 106647.

35. Chemali, E., et al., *Long short-term memory networks for accurate state-of-charge estimation of Li-ion batteries.* IEEE Transactions on Industrial Electronics, 2017. **65**(8): p. 6730-6739.

36. Zhang, Z., et al. *A state-of-charge estimation method based on bidirectional lstm networks for lithium-ion batteries*. in *2020 16th International Conference on Control, Automation, Robotics and Vision (ICARCV)*. 2020. IEEE.

37.   Hong, J., Z. Wang, and Y. Yao, *Fault prognosis of battery system based on accurate voltage abnormity prognosis using long short-term memory neural networks.* Applied Energy, 2019. **251**: p. 113381.

38.   Rafi, S.H., S.R. Deeba, and E. Hossain, *A short-term load forecasting method using integrated CNN and LSTM network.* IEEE Access, 2021. **9**: p. 32436-32448.

39.   Li, C., et al., *Short-term wind speed interval prediction based on ensemble GRU model.* IEEE transactions on sustainable energy, 2019. **11**(3): p. 1370-1380.

40.   Liu, M., P. Qiu, and K. Wei. *Research on wind speed prediction of wind power system based on GRU deep learning.* in *2019 IEEE 3rd Conference on Energy Internet and Energy System Integration (EI2)*. 2019. IEEE.

41.   Liu, X., Z. Lin, and Z. Feng, *Short-term offshore wind speed forecast by seasonal ARIMA-A comparison against GRU and LSTM.* Energy, 2021. **227**: p. 120492.

42.   Xiuyun, G., et al. *Short-term load forecasting model of gru network based on deep learning framework.* in *2018 2nd IEEE Conference on Energy Internet and Energy System Integration (EI2)*. 2018. IEEE.

43.   Song, Y., et al. *Lithium-ion battery remaining useful life prediction based on GRU-RNN*. in *2018 12th international conference on reliability, maintainability, and safety (icrms)*. 2018. IEEE.

44.   Bonfitto, A., *A method for the combined estimation of battery state of charge and state of health based on artificial neural networks.* Energies, 2020. **13**(10): p. 2548.

45.   Kim, T.J., B.D. Youn, and H.J. Kim, *Battery pack temperature estimation model for evs and its semi-transient case study.* Chemical Engineering Transactions, 2013. **33**: p. 955-960.

46.   Kim, U.S., et al., *Modelling the thermal behaviour of a lithium-ion battery during charge.* Journal of Power Sources, 2011. **196**(11): p. 5115-5121.

47.   Guo, M. and R.E. White, *A distributed thermal model for a Li-ion electrode plate pair.* Journal of Power Sources, 2013. **221**: p. 334-344.

48.   Hussein, A.A. and A.A. Chehade, *Robust artificial neural network-based models for accurate surface temperature estimation of batteries.* IEEE Transactions on Industry Applications, 2020. **56**(5): p. 5269-5278.

49.   Feng, F., et al., *Co-estimation of lithium-ion battery state of charge and state of temperature based on a hybrid electrochemical-thermal-neural-network model.* Journal of Power Sources, 2020. **455**: p. 227935.

50.   Steinstraeter, M., J. Buberger, and D. Trifonov, *Battery and Heating Data in Real Driving Cycles.* IEEE Data Port; IEEE: Manhattan, NY, USA, 2020.

51.   *CAN Bus Explained - A Simple Intro [2022].* 2021.

52.   Adermann, J., J. Kreibich, and M. Lienkamp, *Experimental study of energy consumption variation in recurring driving trips.* J. Electr. Eng, 2017. **5**: p. 253-261.

53.   *layer heater*. http://www.temflexcontrols.com/.

54.   Steinstraeter, M., et al., *Controlling cabin heating to improve range and battery lifetime of electric vehicles.* eTransportation, 2022: p. 100181.

55.   Kalkhambkar, V., R. Kumar, and R. Bhakar, *Energy loss minimization through peak shaving using energy storage.* Perspectives in Science, 2016. **8**: p. 162-165.

56.   Wagner, D., et al., *Battery independent regenerative braking using model predictive control with auxiliary power consumers.* Forschung im Ingenieurwesen, 2019. **83**(4): p. 843-852.

57.   *www.leschroniquesdegoliath.com.* November 8, 2022].

58.   Kurmaev, R.K., V. Struchkov, and V. Novak. *Experience in the development of an effective thermal management system for the high-voltage battery of the vehicle.* in *IOP Conference Series: Materials Science and Engineering.* 2020. IOP Publishing.

59.   *What is Lithium Plating?* 2014.

60.   Pesaran, A., S. Santhanagopalan, and G. Kim, *Addressing the impact of temperature extremes on large format li-ion batteries for vehicle applications (presentation).* 2013, National Renewable Energy Lab.(NREL), Golden, CO (United States).

61.   Cunningham, P., M. Cord, and S.J. Delany, *Supervised learning*, in *Machine learning techniques for multimedia.* 2008, Springer. p. 21-49.

62.   Hastie, T., R. Tibshirani, and J. Friedman, *Unsupervised learning*, in *The elements of statistical learning.* 2009, Springer. p. 485-585.

63.   Zhou, X. and M. Belkin, *Semi-supervised learning*, in *Academic Press Library in Signal Processing.* 2014, Elsevier. p. 1239-1269.

64.   *Illustrated Guide to LSTM's and GRU's.* 2018, https://towardsdatascience.com/illustrated-guide-to-lstms-and-gru-s-a-step-by-step-explanation-44e9eb85bf21: https://towardsdatascience.com/illustrated-guide-to-lstms-and-gru-s-a-step-by-step-explanation-44e9eb85bf21.

65.   Krenker, A., J. Bešter, and A. Kos, *Introduction to the artificial neural networks.* Artificial Neural Networks: Methodological Advances and Biomedical Applications. InTech, 2011: p. 1-18.

66.   Ramachandran, P., B. Zoph, and Q.V. Le, *Searching for activation functions.* arXiv preprint arXiv:1710.05941, 2017.

67.   Sharma, S., S. Sharma, and A. Athaiya, *Activation functions in neural networks.* towards data science, 2017. **6**(12): p. 310-316.

68.   Zaremba, W., I. Sutskever, and O. Vinyals, *Recurrent neural network regularization.* arXiv preprint arXiv:1409.2329, 2014.

69.   Tato, A. and R. Nkambou, *Improving adam optimizer.* 2018.

70.   Yu, Y., et al., *A review of recurrent neural networks: LSTM cells and network architectures.* Neural computation, 2019. **31**(7): p. 1235-1270.

71.   Yao, L. and Y. Guan. *An improved LSTM structure for natural language processing.* in *2018 IEEE International Conference of Safety Produce Informatization (IICSPI).* 2018. IEEE.

72.   Wang, Y., W. Liao, and Y. Chang, *Gated recurrent unit network-based short-term photovoltaic forecasting.* Energies, 2018. **11**(8): p. 2163.

73.   Zhao, R., et al., *Machine health monitoring using local feature-based gated recurrent unit networks.* IEEE Transactions on Industrial Electronics, 2017. **65**(2): p. 1539-1548.

74.   Chai, T. and R.R. Draxler, *Root mean square error (RMSE) or mean absolute error (MAE).* Geoscientific Model Development Discussions, 2014. **7**(1): p. 1525-1534.

75. Fonti, V. and E. Belitser, *Feature selection using lasso.* VU Amsterdam research paper in business analytics, 2017. **30**: p. 1-25.
76. Muthukrishnan, R. and R. Rohini. *LASSO: A feature selection technique in predictive modeling for machine learning.* in *2016 IEEE international conference on advances in computer applications (ICACA).* 2016. IEEE.

VITA AUCTORIS

NAME: Shayan Falahat Doost

PLACE OF BIRTH: Tehran, Iran

YEAR OF BIRTH: 2000

EDUCATION: Eastern Mediterranean University, B.SC
                                    (Mechatronics Engineering), Famagusta,
                                    Cyprus, 2021